del Barrio Castro, Tomás; Escribano, Álvaro; Sibbertsen, Philipp

Working Paper

Modeling and forecasting the long memory of cyclical trends in paleoclimate data

Hannover Economic Papers (HEP), No. 722

Provided in Cooperation with:
School of Economics and Management, University of Hannover

Suggested Citation: del Barrio Castro, Tomás; Escribano, Álvaro; Sibbertsen, Philipp (2024) : Modeling and forecasting the long memory of cyclical trends in paleoclimate data, Hannover Economic Papers (HEP), No. 722, Leibniz Universität Hannover, Wirtschaftswissenschaftliche Fakultät, Hannover

This Version is available at:
https://hdl.handle.net/10419/307736

Modeling and Forecasting the Long Memory of Cyclical Trends in Paleoclimate Data

Tomas del Barrio Castro*, Alvaro Escribano† and Philipp Sibbertsen‡

June 12, 2024

Abstract

This paper identifies and estimates the relevant cycles in paleoclimate data of earth temperature, ice volume and CO_2. Cyclical cointegration analysis is used to connect these cycles to the earth eccentricity and obliquity and to see that the earth surface temperature and ice volume are closely connected. These findings are used to build a forecasting model including the cyclical component as well as the relevant earth and climate variables which outperforms models ignoring the cyclical behaviour of the data. Especially the turning points can be predicted accurately using the proposed approach. Out of sample forecasts for the turning points of earth temperature, ice volume and CO_2 are derived.

Keywords: Paleoclimate Cycles · Cyclical Fractional Cointegration · Forecasting Climate Data .

1 Introduction

Anthropogenic climate change is now a days one of the most important global issues on Earth. Compared to the end of the 19th century, the global surface temperature for the end of the 21st century is very likely to rise by 3.3 to 5.7 $°C$ under the worst-case scenario, "very high greenhouse gas emissions scenario" (Intergovernmental Panel on Climate Change, 2021). This scenario implies dramatic consequences on nature and wildlife in terrestrial, wetland, and ocean ecosystems, and on humanity with respect to food and water security, migration, health, higher risk of conflict worldwide, reduction of global economic production, and a possible collapse of the current societal organization.

Climate change is due to exogenous orbital variables during the history of Earth, and partly due to the influence of humanity during the most recent 10,000 to 15,000 years. First, during the 4.5-billion-year history of Earth, climate change was driven by orbital variables which influenced global ice volume, atmospheric carbon dioxide (CO_2) level, and land surface temperature. The atmospheric CO_2 level and land surface temperature are related to melting glaciers and sea ice.

The main three orbital variables which drive Earth's climate (see figures 2) are: (i) changes in the non-circularity of Earth's orbit with a period of 100,000 years, (ii) changes in the tilt of Earth's rotational axis relative to the ecliptic with a period of 41,000 years, and (iii) circular rotation of the rotational axis itself, which changes the season at which Earth's orbit is nearest to the Sun, with a period that is

*Universitat de les Ilies Balears, E-Mail: tomas.barrio@uib.es

†Department of Economics, Universidad Carlos III de Madrid. E-Mail: alvaroe@eco.uc3m.es

‡Corresponding Author. Leibniz University Hannover, School of Economics and Management, Institute of Statistics, Königsworther Platz 1, D-30167 Hannover, Germany. E-Mail: sibbertsen@statistik.uni-hannover.de. Phone: +49-511-762-3783

between 19,000 to 23,000 years. The cycles of those variables (i.e., the Milankovitch cycles) are the most important orbital variables which influence Earth's climate.

The analysis of the time series behaviour of paleoclimate data has attracted much attention in the recent years. Paleoclimate data is data gathered from cores drilled in the Antarctic ice cap measuring the concentration of carbon dioxid and methan as well as the amount of deuterium in the ice as a proxy for ocean temperature and the volume of ice back for about 800.000 years BP. Paillard (2001) connects these values to the Milankovitch orbital cycles on the intensity of solar radiation reaching the earth in different periods. Sources of variation are the eccentricity of the Earth's orbit, the obliquity of the Earth's axis of rotation with respect to the orbital plane and the precession of the rotational axis. Hays et al. (1976) and later reviewed by Maslin (2016) find that major climate changes are due to variations in obliquity and precession.

The connection among theses variables has been intensively investigated. Fischer et al. (1999) found that increases in CO_2 lagged temperature by 600 ± 400 years. Mudelsee (2001) uses parabolic regression analysis to determine phase relations. Kaufmann and Juselius (2013) and Miller (2019) use cointegration modeling whereas Mac Millan and Wohar (2019) apply regression techniques for temperature and CO_2. Davidson et al. (2015) provide an extensive time series modeling excercise for this data looking also for Granger causalities.

In terms of forecasting climate variables, recent econometric techniques include Machine Learning as in Reikard (2021), VAR(p) models with exogenous orbital variables as in Castle and Hendry (2020) and multivariate score-driven models with exogenous orbital variables as in Blazsek and Escribano (2022) and Blazsek and Escribano (2023). Since the influence of humanity on Earth's climate started approximately 10,000 to 15,000 years ago, by commencing agricultural activities such as cultivating plants and livestock (Ruddiman (2005)), Castle and Hendry (2020) and Blazsek and Escribano (2022) show that the climate forecasts since 12.000 years ago depart from the observed climate values (higher temperature, higher CO_2 and lower global ice-volume) and this is partly due to anthropogenic reasons.

Blazsek and Escribano (2023) introduce new regime-switching score-driven ice-age models to capture the abrupt changes observed when climate variables exceed certain threshold values. They consider a score-driven Markov-switching ice-age model and provided empirical evidence of having structural changes in three climate variables. In particular, they found clear asymmetric cyclical reactions during low-persistence periods of rapid increases in CO_2 and temperature versus the other regime of high persistence periods with decreasing values of CO_2 and temperature. Furthermore, they identify alternative regime switching periods by using a temporal Ward's clustering method (score-driven threshold ice-age models). Optimal clustering suggests to have different clusters for each of the three climate variables. Without taken into consideration the extreme climate effects of the most recent 250 years of fossil fuels burned by humanity, they suggest that for the next 5,000 years there must exist some synchronous turning points between the long-run cyclical evolution of the three climate variables, moving to a new period of increasing global ice volume, decreasing atmospheric CO_2 volume, and decreasing Antarctic land surface temperature in the next 5000 years. Therefore, some of the main purposes of this paper is to study the cyclical behavior of those climate variables, evaluate the possible synchronicity of the turning points and study the existence of cointegration at cyclical frequencies, between the climate variables considered and possibly with some of the three orbital variables.

Although it is generally accepted that eccentricity, obliquity and precession are highly cyclical variables driving carbon dioxid as well as temperature and ice volume and thus introducing also strong cycles into these time series the modeling has focused mainly on the properties of the zero frequency of the respective periodogram and therefore ignoring the cyclical behaviour of the data. In fact, we will show that the dominant frequency in those Paleoclimate variables is not the zero frequency, as is common in most economic variables, see Granger (1966), but other cyclical frequencies. As the cycles in these variables are strongly varying we believe it is justified to model them as being stochastic. Therefore, we

investigate how many different cycles are present in the respective variables and identify dominant cycles for all variables. We model the time series behaviour and especially the persistence of cycles. Another though different approach of modelling the cyclical behaviour of the paleoclimate variables can be found in Proietti and Maddanu (2024).

The paper is organized as follows. In section 2 we describe the data in more detail before introducing our methodology and applying it to the paleoclimate data in section 3. Section 4 contains results on cyclical cointegration between the paleoclimate variables and the explanatory variables, section 6 uses these results to build a forecasting model for the paleoclimate variables and section 7 concludes.

2 Paleoclimate Data and their Properties

Part of the data in this paper are obtained from Jennifer L. Castle and David F. Hendry (Castle and Hendry (2020)). We will provide a description of the dependent and explanatory orbital variables. The dependent variables are global ice volume (Ice_t), atmospheric carbon dioxide ($CO_{2,t}$) and Antarctic land surface temperature ($Temp_t$) which are observed from 798,000 years ago to 1000 years ago, with a 1,000-year observation frequency.

These variables are displayed in figure 1. The data looks in all cases highly cyclical and with a possibly common cycle.

The autocorrelation functions decline faster than the corresponding decline of variables that are non-stationary and integrated of order one, $I(1)$. In fact, they indicated the existence of long memory, fractional integration $I(d)$, $0 < d < 1$. Depending on the particular value of d the climate variables are stationary or non-stationary climate variables as we will see in section 3. Clearly, the autocorrelation functions of figure 1 confirm the cyclical behavior observed in the four paleoclimate variables and show evidence of strong persistence and long memory.

The periodograms show peaks away from the zero frequency for all the series, confirming the believe that the series contain cyclical and long memory characteristics, different from typical spectral shapes of economic $I(1)$ variables, see Granger (1966).

Even if those variables are stationary, it is possible to use alternative time series modeling. For example, Kaufmann and Juselius (2013) and Davidson et al. (2015) use vector error correction models (VECM) with full rank VECM models (no reduced rank as in the case of I(1) and cointegrated variables). Alternatively in the stationary situation it is more natural to consider a VAR model in levels with exogenous orbital variables, as in Castle and Hendry (2020), or as was done by Blazsek and Escribano (2022) and Blazsek and Escribano (2023) who consider a multivariate Student-t score-driven model with the exogenous orbital variables of Milankovitch cycles (eccentricity, obliquity and precession), that improves previous dynamic specifications considered.

The graph of the explanatory variables is given in figure 2. They also show as expected a high amount of cyclical behaviour which is though not absolutely regular.

The autocorrelation functions and periodograms of the explanatory variables may not be so instructive but are given for completeness. It is not surprising to see the cyclical as well as persistent behaviour confirmed in these variables as well. Eccentricity with a cycle of 100 thousand years, obliquity with a cycle of 40 thousand years and precession with a cycle of 23 thousand years as they are indicated by the periodograms of figure 2. Eccentricity has a similar cycle as in Temperature, Ice volume and CO_2 and the corresponding peak of the periodogram seems to be at a common frequency.

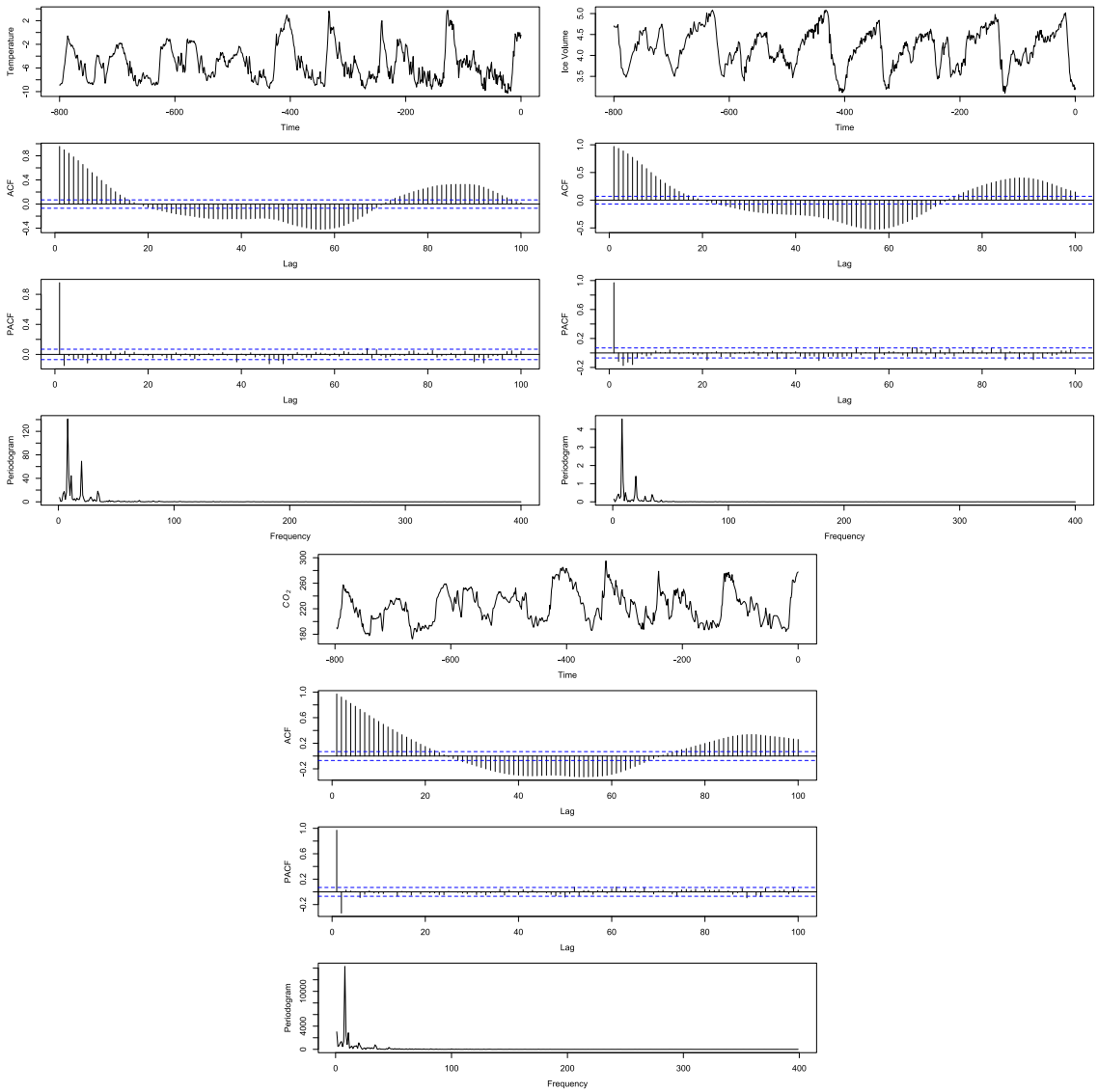

Figure 1: Paleoclimate series, autocorrelation and partial autocorrelation functions and periodograms: Temperature, Ice, CO_2

3 Modeling the Long Memory of the Cyclical Trends of Paleoclimate Data

In order to model the cyclical behavior of the paleoclimate data, we apply the model order selection technique developed in Leschinski and Sibbertsen (2019). The idea of this method is sequentially estimating and filtering the cyclical frequencies of a long-memory time series. The basic idea is as follows: In a first step the maximum of the periodogram is taken and it is tested if this is a significant cyclical peak. Next, the memory parameter at this peak is estimated by local Whittle estimation and the respective Gegenbauer filter is applied to the time series. This procedure is repeated until no significant peak is left.

The model class assumed for the data is the k-factor Gegenbauer model (or GARMA-filter) given by

$$\prod_{a=1}^{k}(1 - 2cos\gamma_a L + L^2)^{d_a} X_t = u_t, \tag{1}$$

where u_t is a linear short-memory process with continuous, bounded and positive spectral density and d_a

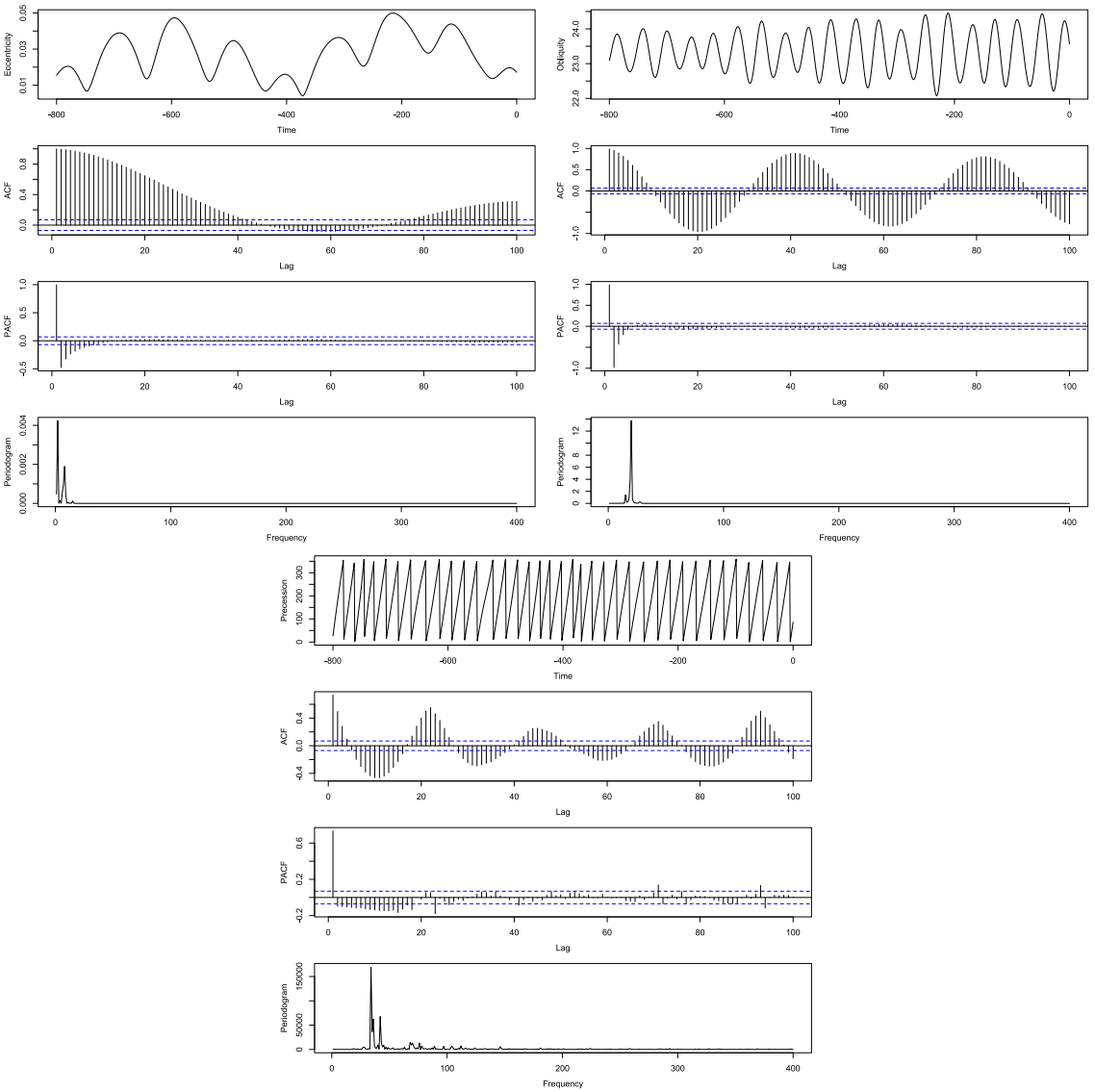

Figure 2: Orbital Series with autocorrelation and partial autocorrelation functions and periodograms: Eccentricity, Obliquity, Precession

is the memory parameter associated with the a-th cyclical frequency γ_a. L denotes the usual lag-operator. The spectral density of model (1) is given by

$$f_X(\lambda) = f_u(\lambda) \prod_{a=1}^{k} |2(cos\lambda - cos\gamma_a)|^{-2d_a}. \tag{2}$$

For $d_a > 0$ the spectral density has poles due to the long memory behaviour at the cyclical frequencies γ_a with $a = 1, \ldots, k$. If u_t is a finite order ARMA process the process (1) coincides with the GARMA-k model of Giraitis and Leipus (1995) which is causal, invertible and has long memory if $|d_a| < 1/2$ $\forall \gamma_a \in (0, \pi)$ and if $|d_a| < 1/4$ $\forall \gamma_a \in \{0, \pi\}$ and it is fractional and nonstationary if $1/2 < d_a < 1$.

Let now the partial parameter vector $\theta_i^0 = (\gamma_1^0, \ldots, \gamma_i^0, d_1^0, \ldots, d_i^0)'$ contain a subset of the true cyclical frequencies γ_a^0 and the respective memory orders d_a^0 at these frequencies for some non-negative integer i and let θ_0 be an empty vector. Further, we denote the Gegenbauer filter by $GG(\gamma_a, d_a) = (1 - 2cos\gamma_a L + L^2)^{d_a}$ and $\Delta(\theta_i) = \prod_{a=1}^{i} GG(\gamma_a, d_a)$. If k^0 is the true order of our process the procedure is motivated by the observation that for $i < k^0$ the filtered process is still a Gegenbauer process but of order $k^0 - i$ and thus with unbounded spectral density. For $i \geq k^0$ the filtered series is short memory having a bounded

spectral density.

To test if there are still any remaining unbounded peaks in the spectral density a modified version of the Walker (1914) g-test is applied. The test statistic is defined as

$$G^* = \max \left\{ \frac{I(\lambda_j)}{\hat{f}(\lambda_j)} \right\} - \log n, \tag{3}$$

where $I(\lambda_j)$ is the periodogram and $\hat{f}(\lambda_j)$ is an estimator of the spectral density detailed in Leschinski and Sibbertsen (2019).

Using this the estimated model order is obtained by

$$\hat{k} = \min_i \{ i \quad \text{such that} \quad G^*(\hat{\theta}_i) < g_{crit}(\alpha) \}, \tag{4}$$

where $g_{crit}(\alpha)$ is the critical value of G^* at the significance level α. A consistent estimator $\hat{\gamma}_a$ for the Gegenbauer frequency γ_a can be obtained by the maximum of the periodogram (see Abadir et al. (2024))

$$\hat{\gamma}_a(\theta_i) = \arg\max_{\lambda_j} I(\lambda_j, \theta_i) \tag{5}$$

and the cyclical local Whittle estimator of Arteche and Robinson (2000) applied to the periodogram of the filtered series can serve as an estimator $\hat{d}_a$ for the memory parameter.

Abadir et al. (2024) suggest an alternative model to the Gegenbauer process applied in our approach. They point out that the distribution of the local Whittle estimator is unknown for an unknown cyclical frequency and thus that the Gegenbauer model requires known cyclical frequencies. In our situation the cycles are driven by geophysical variables and therefore not completely random. Here the specification of the number of relevant frequencies is the more important goal and estimating the relevant frequencies is to some extend of a confirmatory nature. This is why we apply the model selection framework of Leschinski and Sibbertsen (2019) which relies on the Gegenbauer model and use the maximum of the periodogram as an estimator for the cyclical frequency as suggested by Abadir et al. (2024).

Altogether our filtering procedure contains of the following steps:

Step 0: Initialize the procedure with $i = 0$ and set $\hat{\theta}_i$ to be the empty vector θ_0

Step 1: Apply the filter $\Delta_T(\hat{\theta}_i)$ to the time series X_t

Step 2: Test whether there are any significant poles in the spectrum of $\Delta_T(\hat{\theta}_i)X_t$ using the modified G^* test in (3) and proceed to step 3 if the test rejects the null hypothesis that $k^0 = i$ otherwise procede to step 5

Step 3: Estimate γ^0_{i+1} and d^0_{i+1}

Step 4: Increase i by 1 and go back to step 1

Step 5: Estimate k^0 by the estimator (4).

We now apply the above described methodology to our paleoclimate data. We estimate the model order k, this is the number of cyclical frequencies in the data, the frequencies γ_a and the memory parameter d_a for the respective frequency. The results for the paleoclimate variables are given in table 1.

It can be seen that the results are synchronous for the first peak in the periodogram for Temperature and Ice and for CO_2 respectively. For all three series we find a cyclical component at around $\hat{\gamma}_{a_1} = 0.063$. For CO_2 this is the only cyclical component in the model. In all three variables this component is associated with a stationary memory parameter since the parameter $\hat{d}_{a_1}$ is lower than 0.5. The memory is though higher for temperature and ice. For temperature and ice we do find in addition a second cyclical

	Temperature	Ice	CO_2
k	2	2	1
γ_a	0.0628; 0.1509	0.0628; 0.1509	0.063
d_a	0.4221; 0.5219	0.4808; 0.6948	0.3421

Table 1: Results for the paleoclimate variables: Model order (k), cyclical frequencies (γ_a) and memory parameter (d_a)

component at around $\hat{\gamma}_{a_2} = 0.15$. For both variables this component is associated with a non-stationary long memory parameter $\hat{d}_{a_2}$ where $0.5 < \hat{d}_{a_2} < 1$. The component is not present for CO_2.

In order to see, if this cycle can be related to one of our explanatory orbital variables we do the same exercises for these three variables. The results can be found in table 2.

	Eccentricity	Obliquity	Precession
k	5	2	1
γ_a	0.0157; 0.0635; 2.3894; 0.1141; 2.4026	0.1569; 0.2145	0.2667
d_a	0.4987; 0.4547; 0.1; 0.8264; 0.1081	0.9999; 0.9519	0.5171

Table 2: Results for the orbital variables: Model order (k), cyclical frequency (γ_a) and memory parameter (d_a)

For eccentricity we find five cyclical components one of them being the cycle at $\gamma_2 = 0.0635$. It should be noted that this is not the smallest cyclical frequency for eccentricity. The first one is $\gamma_1 = 0.0157$. Thus, the dominant cyclical frequency for the three paleoclimate variables is a long cycle but it is not the zero frequency. Also for eccentricity the cyclical frequency of $\gamma_2 = 0.0635$ is associated with a high but stationary long memory parameter showing that eccentricity also seems to have some irregularities over time. None of the other four frequencies can be found in the paleoclimate variables though.

For obliquity the first cyclical frequency is $\gamma_1 = \hat{\gamma}_{a_2} = 0.1569$ which can be found also in temperature and ice. The $I(1)$ behaviour of obliquity at this frequency may also explain the non-stationarities at temperature and ice at this frequency. Precession has one cyclical component which can be found in neither of the paleoclimate variables.

For all considered variables we tested if the cycles are possibly deterministic rather then stochastic. For this we modeled the cycles with a sinus and cosinus function at the respective frequency and regressed the data on this cycle. After doing so we still found the same cycles in all variables indicating that the cycles are indeed stochastic and not deterministic.

Summarizing, we find that the first cyclical frequency in all paleoclimate variables can be linked to eccentricity creating a cycle of length 100 thousand years. The second cyclical component in temperature and ice can be linked to obliquity creating a cycle of length 40 thousand years. The cycle of precession is of length 23 thousand years.

In order to see if our procedure describes the data well we apply the respective Gegenbauer filter to the paleoclimate time series. The filtered series are given in figure 3 looking much more regular then the original series.

4 Cyclical Fractional Cointegration (Common Cycles)

From the results in the previous section it can be seen that the 100.000 years cycle of eccentricity is also dominant in all paleoclimate variables. Further, Temperature and Ice are also driven by the 40.000 years

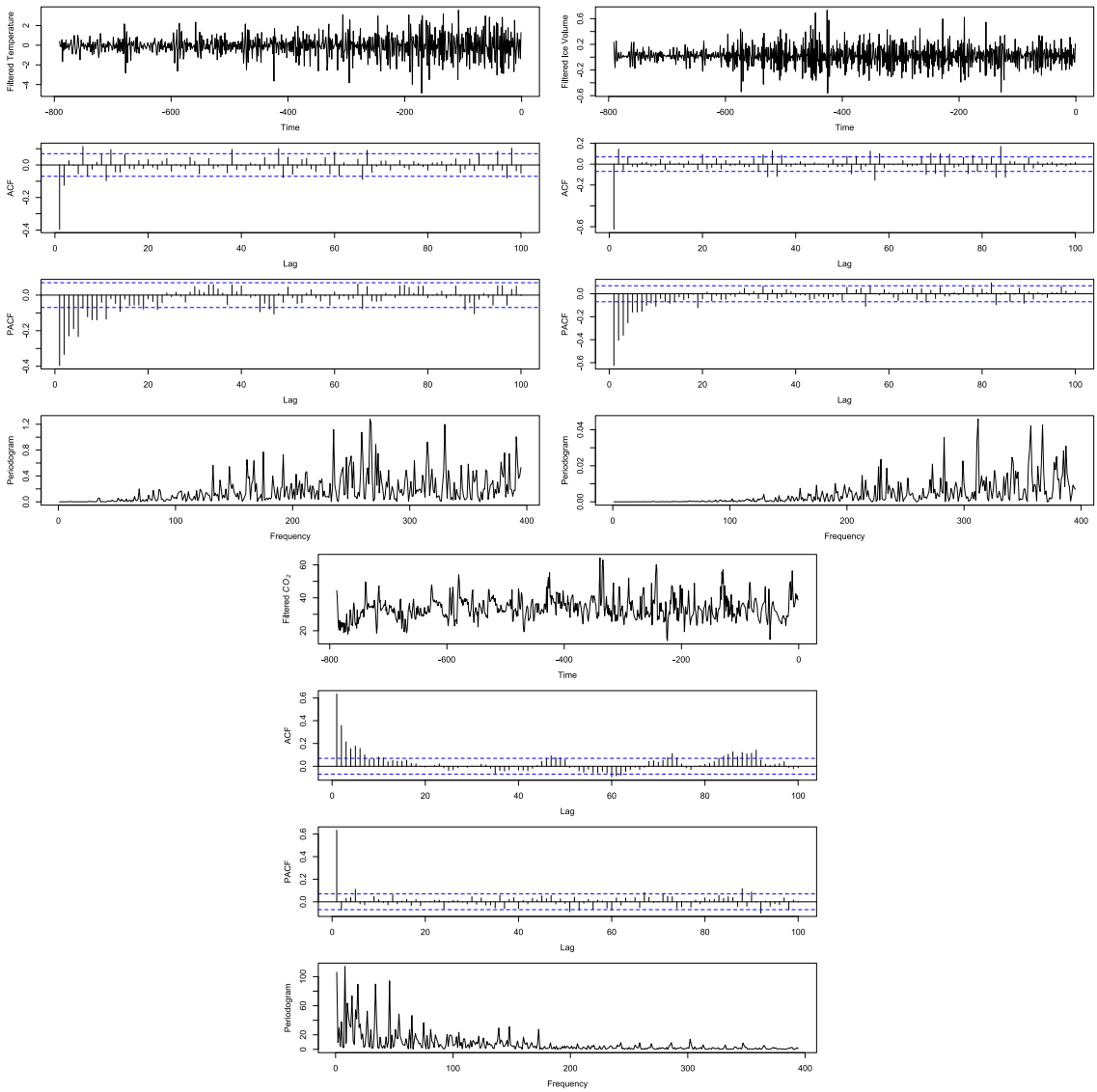

Figure 3: Filtered Series (residuals) and their autocorrelation and partial autocorrelation function and periodogram: Temperature ($\hat{u}_{1t}$), Ice (u_{2t}), CO_2 (u_{3t}) from equation (1)

cycle of obliquity. To get a better understanding on how these variables are connected at the respective cycles we test in this section for cyclical fractional cointegration using the method described in Voges and Sibbertsen (2021).

This approach is again based on the GARMA filter introduced in the previous section. It is general in the sense that it allows cointegration at a specific cyclical frequency γ without assuming cointegration at other frequencies. Further, the cointegration vector β_γ as well as the memory reduction b_γ are frequency-specific. However, cointegration across frequencies is exluded by this approach. The approach assumes the bivariate system

$$BZ_t = \nu_t \qquad \text{with} \qquad B = \begin{pmatrix} 1 & -\beta \\ 0 & 1 \end{pmatrix}, \tag{6}$$

where Z_t is the observed bivariate time series system and ν_t is an unobservable underlying process. By construction all cointegrating relations are subject to the same cointegrating vector $(1, -\beta)$. The first element of ν_t is what is known as the cointegration residuals. In terms of the GARMA filter ν_t can be

written as

$$\nu_t = \begin{pmatrix} \prod_{l_1=1}^{k_1}(1 - cos\gamma_{l_1}L + L^2)^{-(d_{l_1}-b_{l_1})}\varepsilon_{1t} \\ \prod_{l_2=1}^{k_2}(1 - cos\gamma_{l_2}L + L^2)^{-d_{l_2}}\varepsilon_{2t} \end{pmatrix}. \tag{7}$$

If now $\beta \neq 0$ and $b_{l_1} > 0$ the vector Z_t is cointegrated. Note that the cointegration strength b_{l_1} can differ between frequencies.

We test for cointegration by performing a t-test on the null hypothesis $\beta = 0$. The memory parameters as well as the cointegrating vector β are estimated simultaneously by the generalized local Whittle estimator derived in Voges and Sibbertsen (2021). They prove consistency and asymptotic normality of the generalized local Whittle estimator. This result on asymptotic normality is used to construct a t-test on $\beta = 0$.

In this paper we understand fractional cointegration in a wider sense as outlined in Hualde and Nielsen (2023). We do not assume that the memory parameters need to be equal at the respective frequency. We speak of cointegration if the strength of the memory is reduced through the cointegrating relation.

Cointegration may appear at the frequencies $\hat{\gamma}_{a1} = 0.0628$ and $\hat{\gamma}_{a2} = 0.1509$. As our approach can only identify cointegration at one cyclical frequency all other cycles are filtered out of the data before applying our test. We test pairwise all combinations which have the respective frequencies in common as the above described approach is bivariate. We estimate the fractional cointegration parameter β and apply a t-test for the hypothesis $\beta = 0$ at the 5% significance level. We reject the null hypothesis of no cointegration if the absolute value of the test statistic T^* exceeds the critical value of $c = 1.95996$. The bandwidth parameter for the local Whittle estimator was chosen as $m = N^{0.6}$ with N denoting the sample size but the results proved to be robust against other choices. The results for the frequency $\hat{\gamma}_{a2} = 0.1509$ are provided in table 3

	$\hat{\beta}$	T^*	decision	d-b
Temperature - Ice	0.3186	2.3218	cointegration	0.1745
Temperature - Obliquity	0.776	5.6560	cointegration	0.1509
Ice - Obliquity	1.0296	7.5035	cointegration	0.275

Table 3: Results for cointegration at the second common frequency

As can be seen we find cyclical cointegration for all pairs for the 40.000 year cycle. The earths obliquity cycle also drives temperature and ice. In addition there is a cointegrating relation between temperature and ice as well. Here we see that the earth obliquity is responsible for a long-term equlibrium between temperature and ice volume.

The results for the frequency $\hat{\gamma}_{a1} = 0.0628$ are displayed in table 4

	$\hat{\beta}$	T^*	decision	d-b
Temperature - Ice	0.55	4.009	cointegration	0.02
Temperature - CO_2	-0.2156	-1.5711	no cointegration	
Ice - CO_2	-0.0822	-0.5994	no cointegration	
Temperature - Eccentricity	-0.3978	-2.8989	cointegration	0.0180
Ice - Eccentricity	-0.4648	-3.3874	cointegration	0
CO_2 - Eccentricity	-0.6322	-4.6071	cointegration	0

Table 4: Results for cointegration at the second common frequency

For the smaller frequency $\hat{\gamma}_{a1} = 0.0628$ describing the 100.000 year cycle all of the paleoclimate variables

are cointegrated with a negative cointegration parameter with the exogeneous variable Eccentricity. Thus the earth eccentricity drives the cycles of all paleoclimate variabels. In addition to this we find fractional coointegration between temperature and ice with a positive coefficient for this cycle as well. We cannot identify a fractional cointegration relation between temperature or ice and CO_2. For temperature and CO_2 the value of the test statistic is though very close to the critical value for the 10% significance level. Further, we consider a two-sided test rather then a one-sided. So with CO_2 the findings are slightly unsharp. A reason for this might be that CO_2 is lagged to temperature and we also test for contemporaneous cointegration.

It should be once again emphasized that these results are cointegration results for the respective cyclical frequencies after a priori filtering out all other cyclical frequencies. So they may seem counter intuitive from a first glance. For instance it may be expected to have a negative coefficient for the cointegration relation of temperature and ice rather than a positive. However, if we run a regression of temperature on ice at the zero frequency the coefficient becomes significantly negative as expected.

The cycles of the earth precession cannot be found in the paleoclimate variables and thus do not lead to cointegrating relations.

Summarizing our results we have for temperature from the fitted k-factor Gegenbauer model

$$(1 - 2cos(0.0628)L + L^2)^{0.42}(1 - 2cos(0.1509)L + L^2)^{0.52}temp_t = \hat{u}_{1t} \tag{8}$$

and for obliquity we get

$$(1 - 2cos(0.1509)L + L^2)^{0.99}(1 - 2cos(0.2145)L + L^2)^{0.95}ob_t = \hat{u}_{2t}. \tag{9}$$

To test for cyclical cointegration between these two variables we have to a priori filter out the frequency $\gamma_{a1} = 0.0628$ for temperature and $\gamma_{a3} = 0.2145$ for obliquity. This gives the model

$$\begin{aligned} (1 - 2cos(0.1509)L + L^2)^{0.52}\tilde{temp}_t &= \hat{u}_{1t} \\ (1 - 2cos(0.1509)L + L^2)^{0.99}\tilde{ob}_t &= \hat{u}_{2t} \end{aligned} \tag{10}$$

and thus

$$\begin{aligned} \tilde{temp}_t &= (1 - 2cos(0.1509)L + L^2)^{-0.52}\hat{u}_{1t} \\ \tilde{ob}_t &= (1 - 2cos(0.1509)L + L^2)^{-0.99}\hat{u}_{2t}. \end{aligned} \tag{11}$$

Let now in our cointegration setup be

$$z_t = \begin{pmatrix} \tilde{temp}_t \\ \tilde{ob}_t \end{pmatrix} \tag{12}$$

and

$$\begin{pmatrix} 1 & -\beta \\ 0 & 1 \end{pmatrix} \tag{13}$$

we obtain the cyclical cointegration model

$$
\begin{aligned}
Bz_t &= \begin{pmatrix} \tilde{temp}_t - \beta\tilde{o}b_t \\ \tilde{o}b_t \end{pmatrix} \\
&= \begin{pmatrix} (1-2cos(0.1509)L+L^2)^{-0.52}\tilde{u}_{1t} - \beta(1-2cos(0.1509)L+L^2)^{-0.99}\tilde{u}_{2t} \\ (1-2cos(0.1509)L+L^2)^{-0.99}\tilde{u}_{2t} \end{pmatrix} \\
&= \begin{pmatrix} (1-2cos(0.1509)L+L^2)^{-0.15}\hat{\varepsilon}_{1t} \\ (1-2cos(0.1509)L+L^2)^{-0.99}\tilde{u}_{2t} \end{pmatrix}
\end{aligned} \tag{14}
$$

with $\beta = 0.776$ being the cointegration parameter. The t-test for the null hypothesis of no cyclical cointegration which is $\beta = 0$ has a test test statistic of $T^* = 5.656$ which is larger then the 5% critical value of 1.95996 leading to a rejection of the null hypothesis of no cointegration at the frequency 0.1509.

5 Constructing a Forecasting Model

In the last sections we discovered which of the earth variables cycles are relevant for the paleoclimate variables and which are the driving and relevant variables. However, as our cyclical cointegration approach relies on pre-filtering of the not relevant cycles it is not suitable for forecasting earth temperature and ice volume. We therefore need to go an alternative route which is outlined in this section.

5.1 Zero Frequency Long-Memory with a VAR(1).

In Bauwens et al. (2023), extending the results of Chevillon et al. (2018) (see also Schennach (2018)) it was shown that the zero frequency long-memory observed in a univariate time series could be the result of the marginalization of an infinitely large VAR(1) system that satisfies certain specific assumptions. Denote by n the number of time series in the VAR(1) system and t is the time dimension of the system. The n time series in the VAR(1) system are collected in the $n \times 1$ vector $\mathbf{y}_{n,t} = [y_{1,t}, y_{2,t}, \ldots, y_{n,t}]$ and we have the following VAR(1):

$$
(I_n - \mathbf{A}_n L)\,\mathbf{y}_{n,t} = \epsilon_{n,t} \tag{15}
$$

where $\epsilon_{n,t}$ is a $n \times 1$ vector of identically and independently distributed innovations with zero expectation and variance–covariance matrix Σ_n. This variance-covariance matrix Σ_n could be diagonal but it is not a necessary condition. Denote the matrix polynomial in the lag operator $(I_n - \mathbf{A}_n L)$ as $(I_n - \mathbf{A}_n L) = \mathbf{A}_n^0(L)$. Finally $\mathbf{A}_n$ is a $n \times n$ matrix of coefficients. This matrix was defined by Chevillon et al. (2018) as a square Toeplitz matrix. Furthermore, Bauwens et al. (2023) show that if $\mathbf{A}_n$ and the generic entries of the former matrix a_{ij}^n are defined in such a way that the following three conditions hold, for "small" $\varepsilon > 0$ and $\varepsilon' > 0$:

1. The elements of the main diagonal of $\mathbf{A}_n$, that is, a_{ii}^n for $i = 1, 2, \ldots, n$ are close to 1/2 ($a_{ii}^n \in (1/2 - \varepsilon, 1/2]$)
2. The elements outside the main diagonal of $\mathbf{A}_n$, that is, a_{ij}^n for $i \neq j$ are non-negative close to zero and of order $O\left(n^{-1}\right)$ ($0 \leq n a_{ij}^n < \varepsilon\prime$).
3. the sums of the elements of a row and of column of matrix $\mathbf{A}_n$ is equal to 1 ($\sum_{i=1}^n a_{ij}^n = 1$ and $\sum_{j=1}^n a_{ij}^n = 1$),

model (15) is compatible with the presence of long memory in the marginalized time series ($y_{i,t}$ for $i = 1, 2, \ldots, n$) and compatible with the theoretical results of both Chevillon et al. (2018) and Schennach (2018). In particular Bauwens et al. (2023) propose the following definition for $\mathbf{A}_n$ that guarantees the previous three conditions and is compatible too with Chevillon et al. (2018) and Schennach (2018):

$$\begin{aligned}\mathbf{A}_n &= d_0\mathbf{I}_n + \frac{1-d_0}{n-1}\left(\mathbf{J}_n - \mathbf{I}_n\right) \\ &= \frac{d_0 n - 1}{n-1}\mathbf{I}_n + \frac{1-d_0}{n-1}\mathbf{J}_n \\ &= \frac{d_0 n - 1}{n-1}\mathbf{I}_n + \frac{1-d_0}{n-1}1_n \times 1_n',\end{aligned} \tag{16}$$

where d_0 is close to $1/2$, $\mathbf{I}_n$ and $\mathbf{J}_n$ are the identity matrix and a square matrix of ones respectively. Note that $\mathbf{J}_n$ is a circulant matrix of rank one and it is possible to write $\mathbf{J}_n = 1_n \times 1_n'$, where 1_n is a $n \times 1$ vector of ones. Hence for a generic observation of the VAR(1) $y_{i,t}$ (15)-(16) it is possible to write:

$$\begin{aligned}y_{i,t} &= \frac{(d_0 n - 1)}{(n-1)}y_{i,t-1} + \frac{(1-d_0)}{(n-1)}1_n \times 1_n'\mathbf{y}_{n,t-1} + \epsilon_{i,t} \\ &= \frac{(d_0 n - 1)}{(n-1)}y_{i,t-1} + \frac{(1-d_0)\,n}{(n-1)}\bar{y}_{t-1} + \epsilon_{i,t} \\ \bar{y}_t &= \frac{1}{n}1_n'\mathbf{y}_{n,t} = \frac{1}{n}\sum_{i=1}^{n} y_{i,t}.\end{aligned} \tag{17}$$

Hence, as stated by Bauwens et al. (2023) $y_{i,t}$ can be expressed as the weighted average of the idiosyncratic innovation $\epsilon_{i,t}$, the lagged value $y_{i,t-1}$ and the lagged cross-section average $\bar{y}_{t-1}$. This cross-section average or common factor behaves like a random walk for finite n. This fact was shown by Bauwens et al. (2023) as the columns of $\mathbf{A}_n$ sum to unity. Then we could write $1_n' \times \mathbf{A}_n^0(1) = 1_n' \times (I_n - \mathbf{A}_n) = 0$ and $1_n' \times \mathbf{A}_n^0(L) = 1_n' \times (I_n - \mathbf{A}_n L) = (1-L) \times 1_n'$, and hence we can write for $\bar{y}_t$:

$$\begin{aligned}\bar{y}_t &= \bar{y}_{t-1} + \bar{\epsilon}_t \\ \bar{\epsilon}_t &= \frac{1}{n}\sum_{i=1}^{n}\epsilon_{i,t}.\end{aligned} \tag{18}$$

As shown in Bauwens et al. (2023) the variance of the average innovation in (18) $\bar{\epsilon}_t$ decreases as n gets larger, and hence $\bar{y}_t$ correspond to a "damped trend" process $\bar{y}_t = O_p\left(\sqrt{T/n}\right) = o_p(1)$. This "damped trend" process is the source of long memory in the time series of the multivariate VAR(1) model (15).

The previous set-up can be extended to the case of the Nyquist frequency and harmonic frequencies. Another important implication of (17) is that all the marginalized time series of the VAR(1) (15) share a common factor, hence it is clear that we have cointegration between any two time series of (15) and that the cointegration vector will be of the $[1, -1]$ form.

5.2 Nyquist Frequency Long-Memory with a VAR(1)

We define the following VAR(1):

$$\left(I_n + \mathbf{A}_n L\right)\mathbf{y}_{n,t} = \epsilon_{n,t}, \tag{19}$$

with $\mathbf{A}_n$ defined as in (16). Denote the matrix polynomial in the lag operator $(I_n + \mathbf{A}_n L)$ as $(I_n + \mathbf{A}_n L) = \mathbf{A}_n^{\pi}(L)$. Note that now for a marginalized time series of the vector $\mathbf{y}_{n,t}$ it is possible to write:

$$\begin{aligned} y_{i,t} &= -\frac{(d_0 n - 1)}{(n-1)} y_{i,t-1} - \frac{(1-d_0)}{(n-1)} 1_n \times 1_n' \mathbf{y}_{n,t-1} + \epsilon_{i,t} \\ &= -\frac{(d_0 n - 1)}{(n-1)} y_{i,t-1} - \frac{(1-d_0)\, n}{(n-1)} \bar{y}_{t-1} + \epsilon_{i,t} \\ \bar{y}_t &= \frac{1}{n} 1_n' \mathbf{y}_{n,t} = \frac{1}{n} \sum_{i=1}^{n} y_{i,t}. \end{aligned} \tag{20}$$

And as the columns of $\mathbf{A}_n$ sum to unity, we have $1_n' \times \mathbf{A}_n^{\pi}(-1) = 1_n' \times (I_n + \mathbf{A}_n(-1)) = 1_n' \times (I_n - \mathbf{A}_n) = 0$ and $1_n' \times \mathbf{A}_n^{\pi}(L) = 1_n' \times (I_n + \mathbf{A}_n L) = (1+L) \times 1_n'$, and hence we can write for $\bar{y}_t$:

$$\begin{aligned} \bar{y}_t &= -\bar{y}_{t-1} + \bar{\epsilon}_t \\ \bar{\epsilon}_t &= \frac{1}{n} \sum_{i=1}^{n} \epsilon_{i,t}. \end{aligned} \tag{21}$$

Now, if we compare (17) with 20), we move from a positive AR(1) in terms of the lagged $y_{i,t}$ to a negative one. That is we move from the zero to the Nyquist frequency. And now in (20) the "damped" integrated process (21) is associated to the Nyquist frequency.

5.3 Complex value Long-Memory with a VAR(1) associated to Harmonic frequencies.

If we define the following VAR(1):

$$\left(I_n - e^{\pm i\gamma} \mathbf{A}_n L\right) \mathbf{y}_{n,t} = \epsilon_{n,t}, \tag{22}$$

with $\mathbf{A}_n$ defined as in (16), and $e^{\pm i\gamma} = \cos(\gamma) \pm i \sin(\gamma)$, γ is a harmonic frequency such that $\gamma \in (0, \pi)$ and $i = \sqrt{-1}$. Hence, we face a complex value VAR(1). Denote the matrix polynomial in the lag operator $\left(I_n - e^{\pm i\gamma} \mathbf{A}_n L\right)$ as $\left(I_n - e^{\pm i\gamma} \mathbf{A}_n L\right) = \mathbf{A}_n^{\pm\gamma}(L)$. Note that now for a marginalized time series of the vector $\mathbf{y}_{n,t}$ it is possible to write:

$$\begin{aligned} y_{i,t} &= e^{\pm i\gamma} \frac{(d_0 n - 1)}{(n-1)} y_{i,t-1} + e^{\pm i\gamma} \frac{(1-d_0)}{(n-1)} 1_n \times 1_n' \mathbf{y}_{n,t-1} + \epsilon_{i,t} \\ &= e^{\pm i\gamma} \frac{(d_0 n - 1)}{(n-1)} y_{i,t-1} + e^{\pm i\gamma} \frac{(1-d_0)\, n}{(n-1)} \bar{y}_{t-1} + \epsilon_{i,t} \\ \bar{y}_t &= \frac{1}{n} 1_n' \mathbf{y}_{n,t} = \frac{1}{n} \sum_{i=1}^{n} y_{i,t}. \end{aligned} \tag{23}$$

As the columns of $\mathbf{A}_n$ sum to unity, we have $1_n' \times \mathbf{A}_n^{\pm\gamma}\left(e^{\mp i\gamma}\right) = 1_n' \times \left(I_n - e^{\pm i\gamma} \mathbf{A}_n \left(^{\mp i\gamma}\right)\right) = 1_n' \times (I_n - \mathbf{A}_n) = 0$ and $1_n' \times \mathbf{A}_n^{\pm\gamma}(L) = 1_n' \times \left(I_n - e^{\pm i\gamma} \mathbf{A}_n L\right) = \left(1 - e^{\pm i\gamma} L\right) \times 1_n'$, and hence we can write for $\bar{y}_t$:

$$\bar{y}_t = e^{\pm i\gamma}\bar{y}_{t-1} + \bar{\epsilon}_t \tag{24}$$
$$\bar{\epsilon}_t = \frac{1}{n}\sum_{i=1}^{n}\epsilon_{i,t}.$$

Now, if we compare (17) with (23), we move from a positive AR(1) in terms of the lagged $y_{i,t}$ to a complex valued one associated to the harmonic frequency γ. And now in (23) the "damped" integrated process (24) is associated to the harmonic frequency γ.

5.4 Long-Memory with a VAR(2) associated to Harmonic frequencies

Finally to obtain a real value VAR(2) with long-memory for the marginalized time series we need to include both the complex conjugate polynomials of order one and have:

$$\begin{aligned}\left(I_n - e^{-i\gamma}\mathbf{A}_n L\right)\left(I_n - e^{+i\gamma}\mathbf{A}_n L\right)\mathbf{y}_{n,t} &= \epsilon_{n,t} \\ \left(I_n - \left[e^{-i\gamma} + e^{+i\gamma}\right]\mathbf{A}_n L + e^{-i\gamma}e^{+i\gamma}\mathbf{A}_n^2 L\right)\mathbf{y}_{n,t} &= \epsilon_{n,t} \\ \left(I_n - 2\cos(\gamma)\,\mathbf{A}_n L + \mathbf{A}_n^2 L\right)\mathbf{y}_{n,t} &= \epsilon_{n,t}.\end{aligned} \tag{25}$$

In model (25) we assume that $\mathbf{A}_n$ follows (16) and in the case of $\mathbf{A}_n^2$ we have[1] that:

$$\begin{aligned}\mathbf{A}_n^2 &= \left(\frac{d_0 n - 1}{n-1}\mathbf{I}_n + \frac{1-d_0}{n-1}1_n \times 1_n'\right)\left(\frac{d_0 n - 1}{n-1}\mathbf{I}_n + \frac{1-d_0}{n-1}1_n \times 1_n'\right) \\ &\left(\frac{d_0 n - 1}{n-1}\right)^2 \mathbf{I}_n + \left(\frac{1-d_0}{n-1}\right)^2 n\left[1_n \times 1_n'\right] + 2\left(\frac{d_0 n - 1}{n-1}\right)\left(\frac{1-d_0}{n-1}\right)\left[1_n \times 1_n'\right] \\ &= \left(\frac{d_0 n - 1}{n-1}\right)^2 \mathbf{I}_n + \left[\left(\frac{1-d_0}{n-1}\right)^2 n + 2\left(\frac{d_0 n - 1}{n-1}\right)\left(\frac{1-d_0}{n-1}\right)\right]\left[1_n \times 1_n'\right] \\ &= \left(\frac{d_0 n - 1}{n-1}\right)^2 \mathbf{I}_n + \left(\frac{n\left(1-d_0^2\right) - 2 + 2d}{(n-1)^2}\right)\left[1_n \times 1_n'\right].\end{aligned} \tag{26}$$

Hence based on (25), (16) and (26) it is possible to write for a marginalized time series of the vector $\mathbf{y}_{n,t}$:

$$\begin{aligned}y_{i,t} &= 2\cos(\gamma)\frac{(d_0 n - 1)}{(n-1)}y_{i,t-1} + 2\cos(\gamma)\frac{(1-d_0)}{(n-1)}1_n \times 1_n'\mathbf{y}_{n,t-1} \\ &- \left(\frac{d_0 n - 1}{n-1}\right)^2 y_{i,t-2} - \left(\frac{n\left(1-d_0^2\right) - 2 + 2d}{(n-1)^2}\right)1_n \times 1_n'\mathbf{y}_{n,t-2} + \epsilon_{i,t} \\ &= 2\cos(\gamma)\frac{(d_0 n - 1)}{(n-1)}y_{i,t-1} + 2\cos(\gamma)\frac{(1-d_0)\,n}{(n-1)}\bar{y}_{t-1} \\ &- \left(\frac{d_0 n - 1}{n-1}\right)^2 y_{i,t-2} - \left(\frac{n\left(1-d_0^2\right) - 2 + 2d}{(n-1)^2}\right)n\bar{y}_{t-2} + \epsilon_{i,t}\end{aligned} \tag{27}$$

$$\begin{aligned}y_{i,t} &= 2\cos(\gamma)\frac{(d_0 n - 1)}{(n-1)}y_{i,t-1} + 2\cos(\gamma)\frac{(1-d_0)\,n}{(n-1)}\bar{y}_{t-1} \\ &- \left(\frac{d_0 n - 1}{n-1}\right)^2 y_{i,t-2} - \frac{\left(1-d_0^2\right)n}{(n-1)}\bar{y}_{t-2} + \epsilon_{i,t} + o_p(1).\end{aligned} \tag{28}$$

[1] Note that in (26) we use the fact that $1_n \times 1_n'$ is a circulant matrix with all its elements equal to one and we have that $\left(1_n \times 1_n'\right)\left(1_n \times 1_n'\right) = n\left(1_n \times 1_n'\right)$.

If we denote the polynomial in the lag operator in (25) as $\mathbf{A}_{n_2}^{\gamma}(L) = \left(I_n - 2\cos(\gamma)\mathbf{A}_n L + \mathbf{A}_n^2 L^2\right)$ it is possible to see that $1_n' \times \mathbf{A}_{n_2}^{\gamma}\left(e^{\pm i\gamma}\right) = 1_n' \times 0$[2] and also that $1_n' \times \mathbf{A}_{n_2}^{\gamma}(L) = 1_n' \times \left(I_n - 2\cos(\gamma)\mathbf{A}_n L + \mathbf{A}_n^2 L^2\right) = \left(1_n' - 2\cos(\gamma) L 1_n' + L^2 1_n'\right) = 1_n'\left(1 - 2\cos(\gamma) L + L^2\right)$. Hence, as we have that $1_n' \times \mathbf{A}_{n_2}^{\gamma}\left(e^{\pm i\gamma}\right) = 0$ and $1_n' \times \mathbf{A}_{n_2}^{\gamma}(L) = 1_n'\left(1 - 2\cos(\gamma) L + L^2\right)$ it is possible to say that the damped trend $\bar{y}_t$ will behave like a non-stationary process integrated at the frequency γ. That is, we can write:

$$\left(1 - 2\cos(\gamma) L + L^2\right)\bar{y}_t = \bar{\epsilon}_t. \tag{29}$$

Finally, in the case of the VAR(2) (25) it is clear from (28) that all the marginalized time series of the VAR(2) share the common behavior of the damped trend associated to the harmonic frequency γ. Hence any two time series of the VAR(2) are cointegrated with vector $[1, -1]$. That is, we have contemporaneous cointegration between processes with cyclical long memory as in the methodology proposed by Voges and Sibbertsen (2021).

5.5 Monte Carlo Experiment

We run a Monte Carlo Experiment with $n = 1601$ and $T = 4000$ replications with $d_0 = 0.499$ for the process (25) and A_n as in (16) and (26) for $\gamma = \pi/30$.

We do the same for a VAR(2) with $\mathbf{A}_n$ defined as in example 1 in Chevillon et al. (2018)(see also expressions (27) and (28) in the Monte Carlo Section of Bauwens et al. (2023) and figure 2 in Chevillon et al. (2018)). In Figure 4 we collect the results on the average autocorrelation function (ACF), the average partial autocorrelation funcion (PACF) and the average periogram of the first marginalized time series $y_{1,t}$ from the VAR(2) model (25).

From Figure 4, we have evidence of a long-memory behavior in $y_{1,t}$ associated to the frequency $\gamma = \pi/30$. In figure 5 we present also the average correlogram and periodogram of the residuals from a regression with $y_{1,t}$ as dependent variable and $y_{2,t}$ as explanatory variable.

Figure 5 shows that the residuals do not seem to have long-memory. That is in figure 5 we have a pattern compatible with a stationary AR(2) process. Hence, it seems that the long-memory behavior is common between $y_{1,t}$ and $y_{2,t}$. The source of the long memory behavior present in $y_{1,t}$ and $y_{2,t}$ and for all the marginalized time series of the VAR(2) is the damped trend $\left(1 - 2\cos(\gamma) L + L^2\right)\bar{y}_t = \bar{\epsilon}_t$. Clearly any of the time series of the VAR(2) are cointegrated with any of the remaining time series of the VAR(2), as they share a common damped trend $\bar{y}_t$ (that is, $\left(1 - 2\cos(\gamma) L + L^2\right)\bar{y}_t = \bar{\epsilon}_t$). This situation will be more clearly shown when we present the results of the test proposed by Voges and Sibbertsen (2021). This allows us to test for cointegration between time series with a cyclical long-memory behavior[3].

In figure 6 we present the average correlogram and periodogram of the residuals of a regression of $y_{2,t}$ on $y_{2,t-1}$, $y_{1,t-1}$ and $y_{1,t-2}$. That is, we use $y_{2,t}$ and $y_{2,t-1}$ as an approximation of $\bar{y}_{t-1}$ and $\bar{y}_{t-2}$ in (27) and also two lags of $y_{1,t}$ ($y_{1,t-1}$ and $y_{1,t-2}$) to deal with the stationary AR(2) in the process followed by the marginalized time series of the VAR(2). So, we use $y_{1,t} = \beta_0 y_{2,t} + \beta_1 y_{2,t-1} + \beta_2 y_{1,t-1} + \beta_3 y_{1,t-2} + u_t$ which is similar to our forecasting equation in the following section.

From Figure 6, we have evidence that the residuals of our forecasting equation are almost free from serial

[2]Note that we have $1_n' \times \mathbf{A}_{n_2}^{\gamma}\left(e^{\pm i\gamma}\right) = 1_n' \times \mathbf{A}_{n_2}^{\gamma}\left(e^{\pm i\gamma}\right) = 1_n' \times \left(I_n - 2\cos(\gamma)\mathbf{A}_n e^{\pm i\gamma} + \mathbf{A}_n^2 e^{\pm i2\gamma}\right) = \left(1_n' - 2\cos(\gamma) e^{\pm i\gamma} 1_n' + e^{\pm i2\gamma} 1_n' \mathbf{A}_n\right) = \left(1_n' - 2\cos(\gamma) e^{\pm i\gamma} 1_n' + e^{\pm i2\gamma} 1_n'\right) = 1_n'\left(1 - 2\cos(\gamma) e^{\pm i\gamma} + e^{\pm i2\gamma}\right) = 1_n'\left(1 - 2\cos(\gamma)\left[\cos(\gamma) \pm i\sin(\gamma)\right] + \left[\cos(2\gamma) \pm i\sin(2\gamma)\right]\right) = 1_n'\left(\left[1 - 2\cos(\gamma)^2 + \cos(2\gamma)\right] \mp i\left[2\cos(\gamma)\sin(\gamma) - \sin(2\gamma)\right]\right) = 1_n' \times 0$. As we know for the double angle sinus and cosinus formulas that $\sin(2\gamma) = 2\cos(\gamma)\sin(\gamma)$ and $\cos(2\gamma) = \cos(\gamma)^2 - \sin(\gamma)^2$. Hence we have that $2\cos(\gamma)\sin(\gamma) - \sin(2\gamma) = 0$ and also $1 - 2\cos(\gamma)^2 + \cos(2\gamma) = 1 - 2\cos(\gamma)^2 + \cos(\gamma)^2 - \sin(\gamma)^2 = 1 - \cos(\gamma)^2 - \sin(\gamma)^2 = 0$.

[3]Note that in the periodograms of figure 5 we observe a peak at frequency $\pi/30$ as in figure 4 but if we compare the scale of both pictures, the peaks in figure 5 are almost irrelevant compared to the peaks in figure 4. This situation also happens for figure 6.

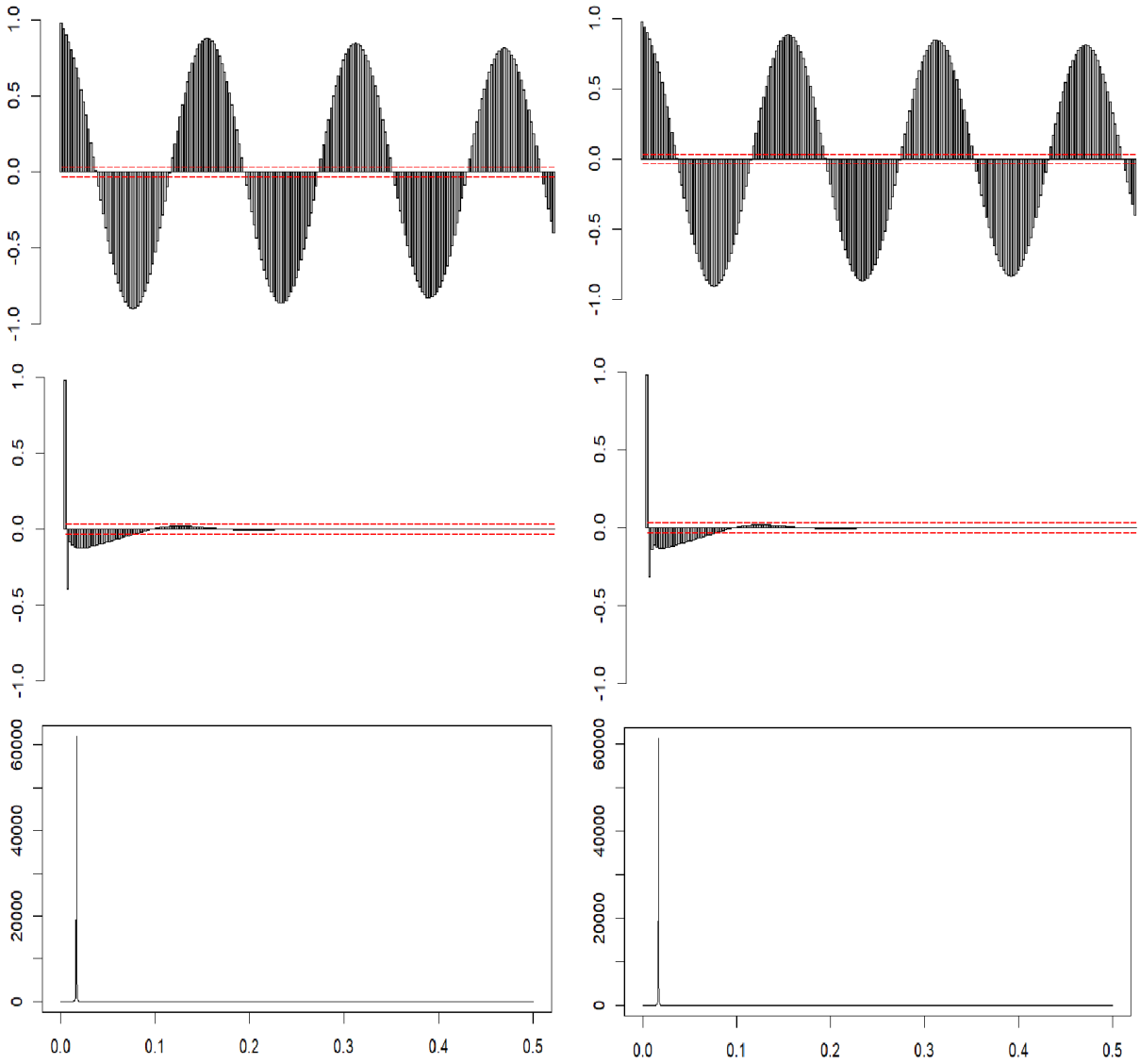

Figure 4: ACF, PACF and periodogram of $y_{1,t}$ following the VAR(2) (25) with $\mathbf{A}_n$ from (16) on the left and $\mathbf{A}_n$ from example 1 Chevillon et al. (2018) on the right

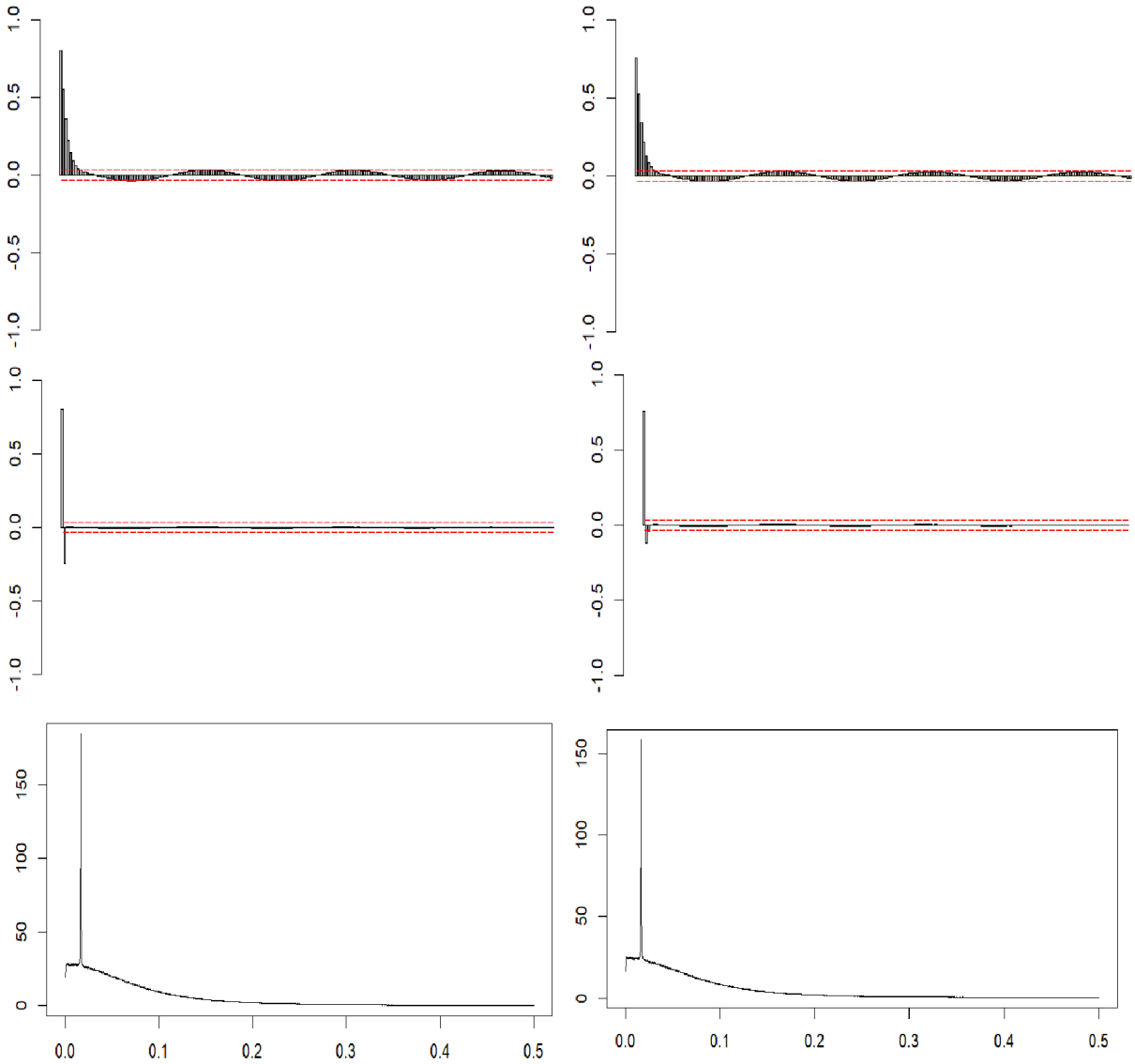

Figure 5: ACF, PACF and periodogram for the residuals from $y_{1,t} = \beta y_{2,t} + u_t$ following the VAR(2) (25) with $\mathbf{A}_n$ (16) on the left and $\mathbf{A}_n$ from example 1 Chevillon et al. (2018) on the right

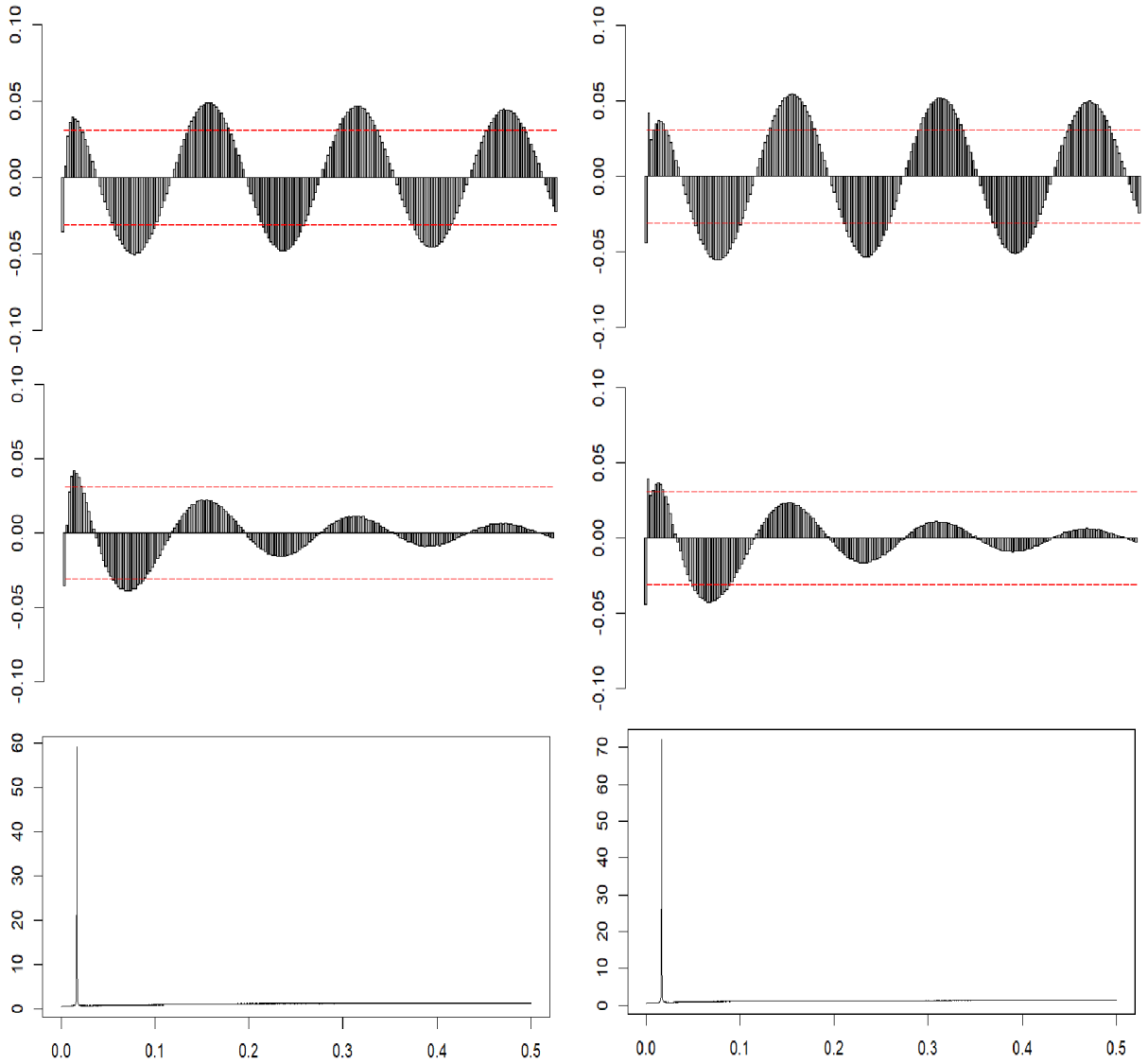

Figure 6: ACF, PACF and periodogram for the residuals from $y_{1,t} = \beta_0 y_{2,t} + \beta_1 y_{2,t-1} + \beta_2 y_{1,t-1} + \beta_3 y_{1,t-2} + u_t$ following the VAR(2) (25) with $\mathbf{A}_n$ (16) on the left and $\mathbf{A}_n$ from example 1 in Chevillon et al. (2018) on the right

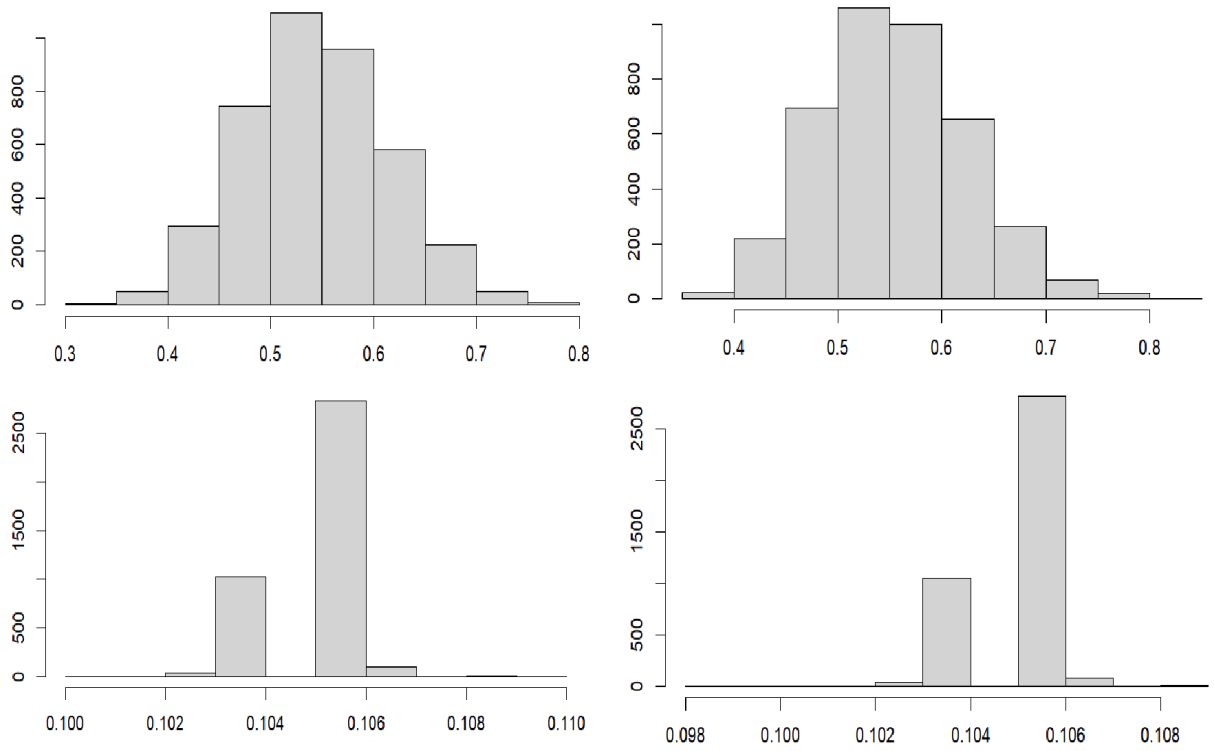

Figure 7: Histogram for the estimator of d and the frequency from Leschinski and Sibbertsen (2019) for a VAR(2) from (25) with $\mathbf{A}_n$ from (16) on the left hand site and with $\mathbf{A}_n$ from example 1 in Chevillon et al. (2018) on the right hand site

correlation, that is, by adding lags of $y_{1,t}$ and $y_{2,t}$, we are able to deal with almost all the remaining serial correlation observed in figure 5.

Figure 7 collects the histograms of the estimations of d and the frequency γ for the marginalized time series $y_{1,t}$, using the methodology proposed by Leschinski and Sibbertsen (2019). Note that the frequency is properly estimated as $\pi/30 \simeq 0.10472$ and that the estimation of the memory parameter d in $\left(1 - 2\cos(\gamma) L + L^2\right)^d y_{1,t} = v_t$ ranges between 0.3 and 0.8. It is centered around 0.55.

Finally, in figure 8 we collect the histograms of the estimators of the cointegration test and the estimation of β after we applied the cointegration methodology developed by Voges and Sibbertsen (2021). In particular we applied Voges and Sibbertsen (2021) methodology when it is applied to $y_{1,t}$ and $y_{2,t}$. Clearly the estimations of β are very close to 1, as it could be expected if we pay attention to expression (28). It shows that with the test of cointegration we always reject the null of no cointegration between $y_{1,t}$ and $y_{2,t}$. Note that the critical value is $c = 1.96$. The proportion of time that we reject the null is 100%.

6 Empirical Modeling and Forecasting of Paleoclimate Cyclical Trends

6.1 In-Sample Forecasts

The previous section showed that a marginalized VAR(2) model is able to approximate cyclical long memory and replicates cyclical cointegration. Therefore, interpreting earth climate as a high dimensional system we approximate the findings on cyclical long memory and cointegration in the paleoclimate and earth variables as a VAR(2) model. To make the model feasible for forecasting we include the cycle as

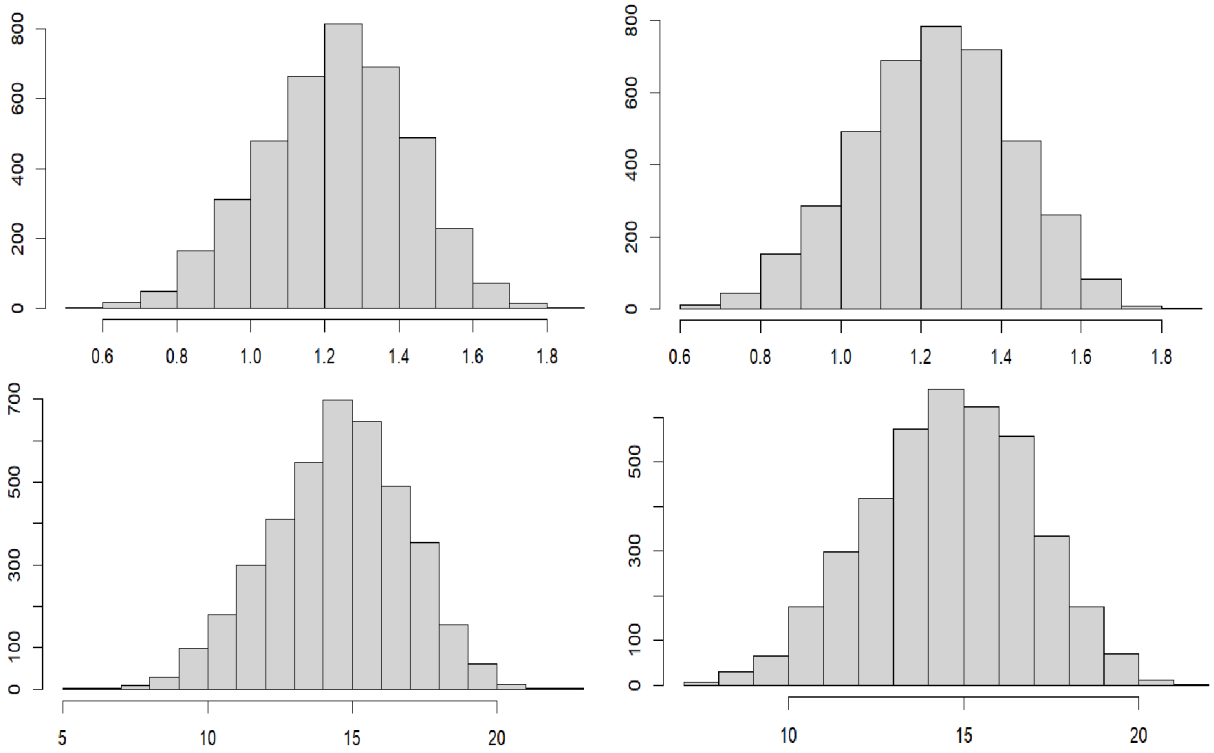

Figure 8: Histogram for the estimator of β and the test statistic from Voges and Sibbertsen (2021) for a VAR(2) from (25) with $\mathbf{A}_n$ from (16) on the left hand site and with $\mathbf{A}_n$ from example 1 inChevillon et al. (2018) on the right hand site

a deterministic sinus and cosinus function as it is common for modeling non stochastic cycles. Point of departure is a reduced form VAR(2) model containing all possibly relevant variables.

$$
\begin{aligned}
\begin{pmatrix} temp_t \\ ice_t \\ CO2_t \end{pmatrix} &= \begin{pmatrix} \alpha_{01} \\ \alpha_{02} \\ \alpha_{03} \end{pmatrix} + \begin{pmatrix} \alpha_{11}(1) & \alpha_{12}(1) & \alpha_{13}(1) \\ \alpha_{21}(1) & \alpha_{22}(1) & \alpha_{23}(1) \\ \alpha_{31}(1) & \alpha_{32}(1) & \alpha_{33}(1) \end{pmatrix} \begin{pmatrix} temp_{t-1} \\ ice_{t-1} \\ CO2_{t-1} \end{pmatrix} \\
&+ \begin{pmatrix} \alpha_{11}(2) & \alpha_{12}(2) & \alpha_{13}(2) \\ \alpha_{21}(2) & \alpha_{22}(2) & \alpha_{23}(2) \\ \alpha_{31}(2) & \alpha_{32}(2) & \alpha_{33}(2) \end{pmatrix} \begin{pmatrix} temp_{t-2} \\ ice_{t-2} \\ CO2_{t-2} \end{pmatrix} \\
&+ \begin{pmatrix} \beta_{10} \\ \beta_{20} \\ \beta_{30} \end{pmatrix} ob_t + \begin{pmatrix} \beta_{11} \\ \beta_{21} \\ \beta_{31} \end{pmatrix} ob_{t-1} + \begin{pmatrix} \gamma_{10} \\ \gamma_{20} \\ \gamma_{30} \end{pmatrix} ecc_t + \begin{pmatrix} \gamma_{11} \\ \gamma_{21} \\ \gamma_{31} \end{pmatrix} ecc_{t-1} \\
&+ \begin{pmatrix} \eta_{10} \\ \eta_{20} \\ \eta_{30} \end{pmatrix} pre_t + \begin{pmatrix} \eta_{11} \\ \eta_{21} \\ \eta_{31} \end{pmatrix} pre_{t-1} \\
&+ \begin{pmatrix} \phi_{11} & \phi_{12} \\ \phi_{21} & \phi_{22} \\ \phi_{31} & \phi_{32} \end{pmatrix} \begin{pmatrix} sin(\gamma_{a1}t) \\ cos(\gamma_{a1}t) \end{pmatrix} + \begin{pmatrix} \varphi_{11} & \varphi_{12} \\ \varphi_{21} & \varphi_{22} \\ \varphi_{31} & \varphi_{32} \end{pmatrix} \begin{pmatrix} sin(\gamma_{a2}t) \\ cos(\gamma_{a2}t) \end{pmatrix} + \begin{pmatrix} \varepsilon_{tempt} \\ \varepsilon_{icet} \\ \varepsilon_{CO2t} \end{pmatrix}
\end{aligned}
\tag{30}
$$

with $\begin{pmatrix} \varepsilon_{tempt} \\ \varepsilon_{icet} \\ \varepsilon_{CO2t} \end{pmatrix} \sim (\mathbf{0}, \begin{pmatrix} \sigma_1^2 & \sigma_{12} & \sigma_{13} \\ \sigma_{12} & \sigma_2^2 & \sigma_{23} \\ \sigma_{31} & \sigma_{32} & \sigma_3^2 \end{pmatrix})$ and $\mathbf{0}$ again denoting the 3×1 vector of zeros.

From this reduced form VAR(2) we end up estimating the following structural form VAR(2) model given by equation (31), applying a general to specific selection procedure with white noise errors. Denoting with $\Delta ecc_t = (1-L)ecc_t$ the first difference of eccentricity the parameter estimates are

$$\begin{aligned}
\hat{temp}_t &= \underset{(1.821)}{^{-8.11}} + \underset{(0.0372)}{^{0.9274}} temp_{t-1} - \underset{(0.0371)}{^{0.1378}} temp_{t-2} - \\
&- \underset{(0.0304)}{^{1.945}} ice_t + \underset{(0.2957)}{^{1.428}} ice_{t-1} + \underset{(0.0532)}{^{0.3064}} ob_t + \\
&+ \underset{(53.422)}{^{221.2246}} \Delta ecc_t + \underset{(0.0027)}{^{0.0088}} CO2_{t-1} \\
\hat{ice}_t &= \underset{(0.1475)}{^{1.3725}} - \underset{(0.0063)}{^{0.0208}} cos(\gamma_1 t) + \underset{(0.0062)}{^{0.0108}} cos(\gamma_2 t) + \underset{(0.0151)}{^{0.8237}} ice_{t-1} - \underset{(0.002)}{^{0.0236}} temp_t - \\
&- \underset{(0.0516)}{^{0.1228}} ob_t + \underset{(0.0526)}{^{0.0904}} ob_{t-1} - \underset{(6.1217)}{^{7.5686}} \Delta ecc_t \\
\hat{CO2}_t &= \underset{(9.482)}{^{62.5923}} + \underset{(0.2427)}{^{0.6354}} cos(\gamma_1 t) + \underset{(0.199)}{^{3.0829}} temp_t - \underset{(0.291)}{^{0.829}} temp_{t-1} - \underset{(0.2297)}{^{0.9251}} temp_{t-2} - \\
&- \underset{(3014)}{^{0.9798}} ob_t + \underset{(0.035)}{^{1.0178}} CO2_{t-1} - \underset{(0.0324)}{^{0.1637}} CO2_{t-2}
\end{aligned} \tag{31}$$

with an adjusted R^2 of $\bar{R}^2 = 0.9284$ for temperature, of $\bar{R}^2 = 0.961$ for ice and an adjusted R^2 of $\bar{R}^2 = 0.9697$ for CO_2. Estimating the model parameters in a VAR system does not significantly change the results. We further applied the White heteroscedasticity test to the residuals of all three regressions. In neither case we can reject the null hypothesis of homoscedasticity. The model contains the first differences of eccentricity for temperature and ice. Examining the first difference of eccentricity shows the same cycle as eccentricity itself as taking first differences does not change the cyclical behavior. We included the first difference of eccentricity to our model as the parameters for the contemporaneous eccentricity and the first lag of eccentricity are almost equal when including both separately. When including the first difference of eccentricity the lag of eccentricity becomes insignificant. This shows that really change of eccentricity is what is driving the paleoclimate variables rather then the level of eccentricity itself.

Our model fitted to the data is depicted in figure 9 for temperature, in figure 10 for ice and in figure 11 for CO_2. The original series is given in black and the fitted model in red. Below the model fit the residual series is plotted. It can be seen that our model provides a close fit to the original data.

We compare the forecasting performance of our model with the baseline model of Castle and Hendry (2020) which has also been used in Blazsek and Escribano (2022). They applied the model

$$\begin{aligned}
\hat{temp}_t &= -2.49 + 0.879 temp_{t-1} + 0.008 CO2_{t-1} - 301 ecc_t \\
&+ 22.6 eccob_t - 9.8 eccob_{t-1} + 25.5 eccpre_t \\
\hat{ice}_t &= 1.43 + 0.86 ice_{t-1} - 0.02 temp_{t-1} + 102 ecc_t \\
&- 101 ecc_{t-1} - 0.04 ob_{t-1} \\
&- 5.07 eccob_t + 5.05 eccob_{t-1} - 4.97 eccpre_t \\
\hat{CO2}_t &= 218 + 0.853 CO2_{t-1} + 1.34 temp_{t-1} + 1400 ecc_t - 3070 ecc_{t-1} - 13 ob_{t-1} + \\
&+ 70.7 eccob_{t-1} + 0.232 ob_t^2
\end{aligned} \tag{32}$$

The two approaches differ clearly. The regression of Castle and Hendry does not include contemporaneous values of temperature on ice volume and of ice volume on temperature. In addition Castle and Hendry include the product of eccentricity and obliquity and the product of eccentricity and precession. The regression for temperature does not include obliquity as a single variable and the regression for ice does

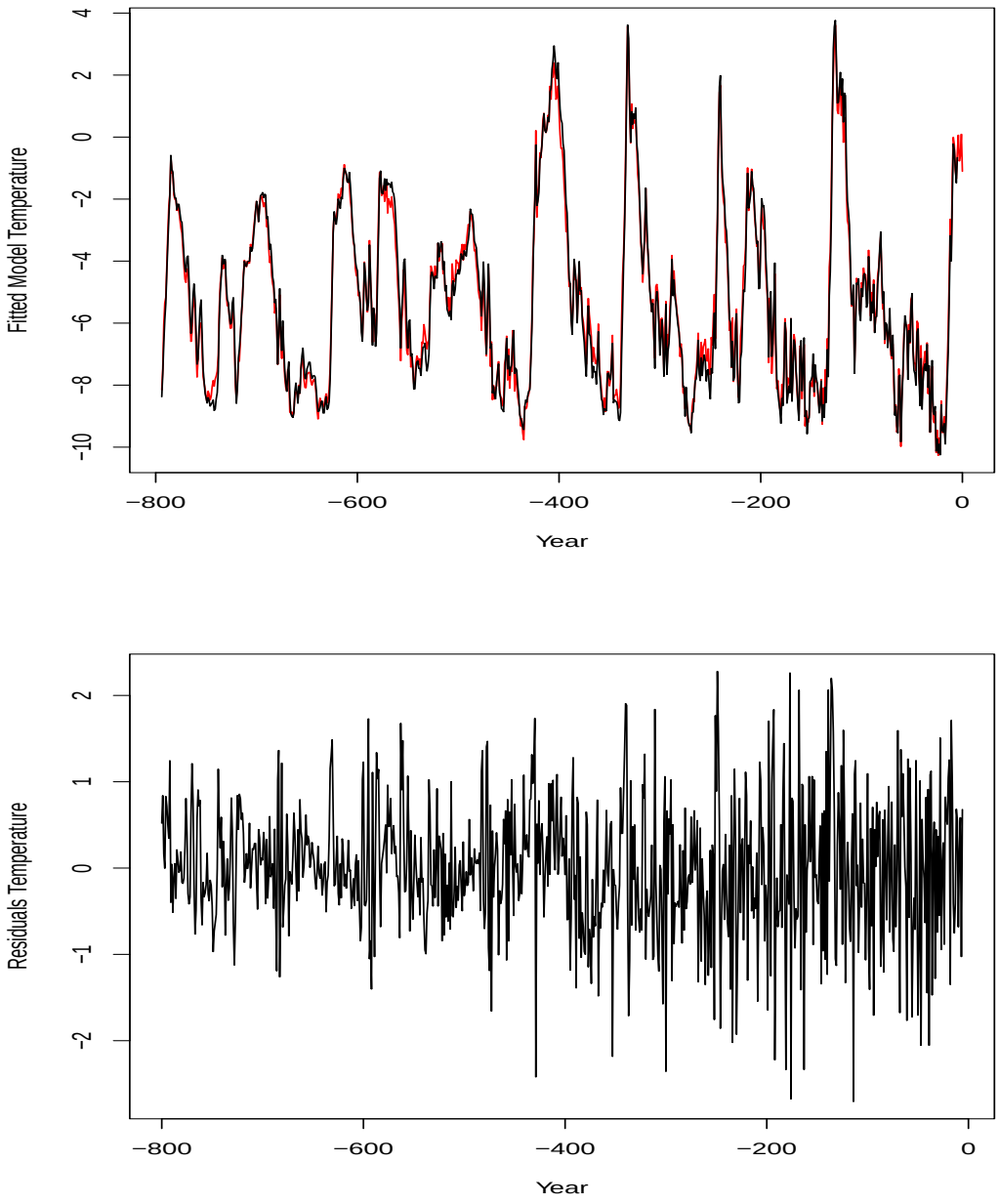

Figure 9: Original Data Temperature (black), fitted model for temperature (red) and regression residuals

not have contemporaneous values of obliquity as explanatory variable. In our regression all variables only have a linear impact and precession is not included.

In order to see if the regression models are well specified we apply the Ljung-Box test to both models testing the null hypothesis that the regression residuals are white noise.

Applying the Ljung-Box test to the residuals of our regression shows the good fit of our model. For ice volume the Ljung-Box test cannot reject the null hypothesis of white noise residuals with a p-value of $p = 0.8262$. For temperature the Ljung-Box test does not reject the null hypothesis of white noise residuals either and has a p-value of 0.8649 and for CO_2 the test has a p-value of $p = 0.8595$ not rejecting the null of white noise residuals again. For the competing model the Ljung-Box test clearly rejects the hypothesis of independent residuals for temperature and CO_2. Castle and Hendry (2020) are aware of

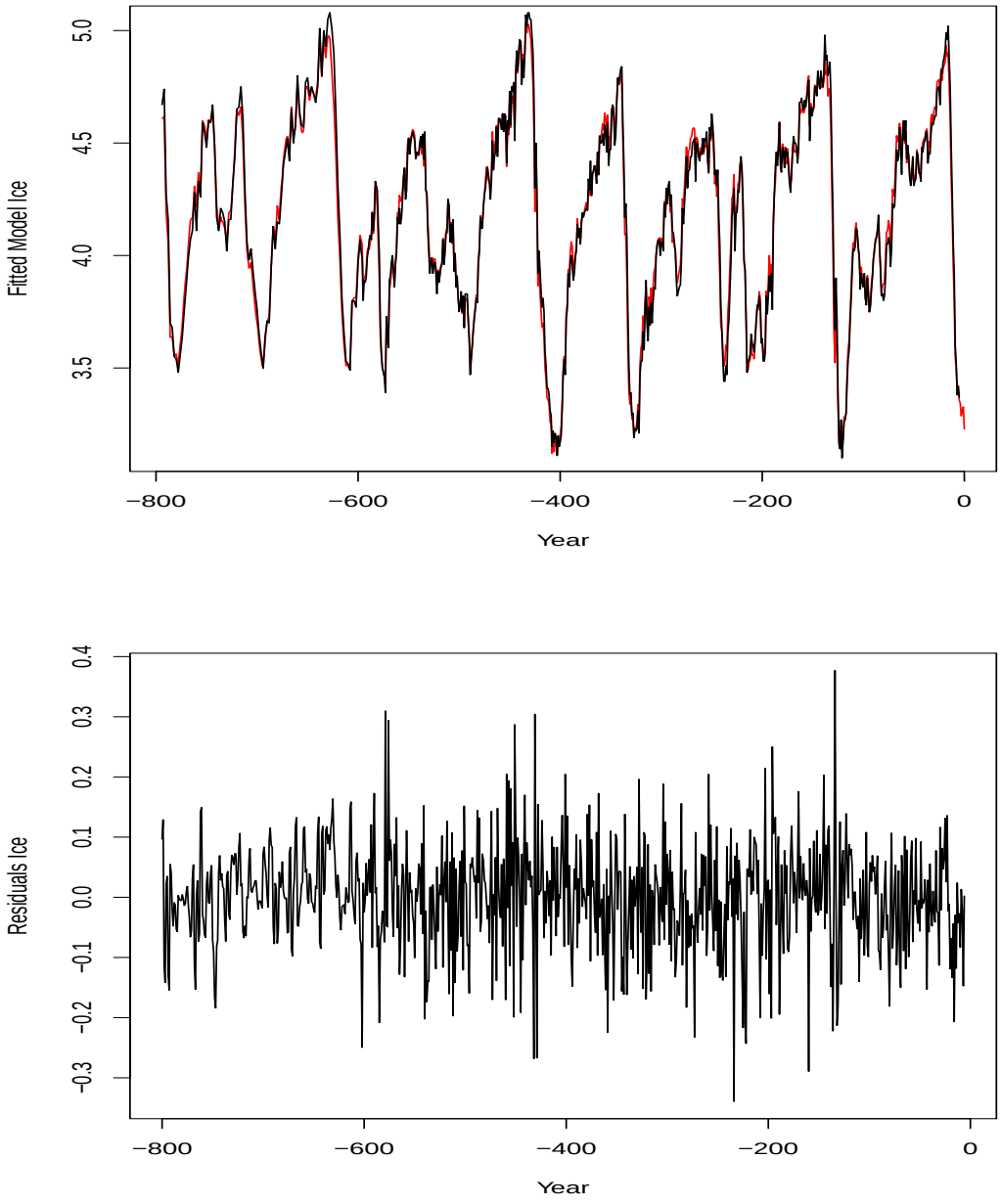

Figure 10: Original Data Ice (black), fitted model for ice (red) and regression residuals

the autocorrelation and mention that to solve it it might need a VAR(2) instead of a VAR(1). In fact, we saw that a VAR(2) represents better the cyclical behavior observed in paleoclimate variables. The p-values are displayed in table 5.

	Cyclical Model	Castle and Hendry
Temperature	0.8649	9.73510^{-7}
Ice	0.8262	0.2595
CO_2	0.8595	$2.2\text{x}10^{-16}$

Table 5: p-values of Ljung-Box test

In a first exercise we give in sample forecasts for our model with a forecasting horizon until the end of

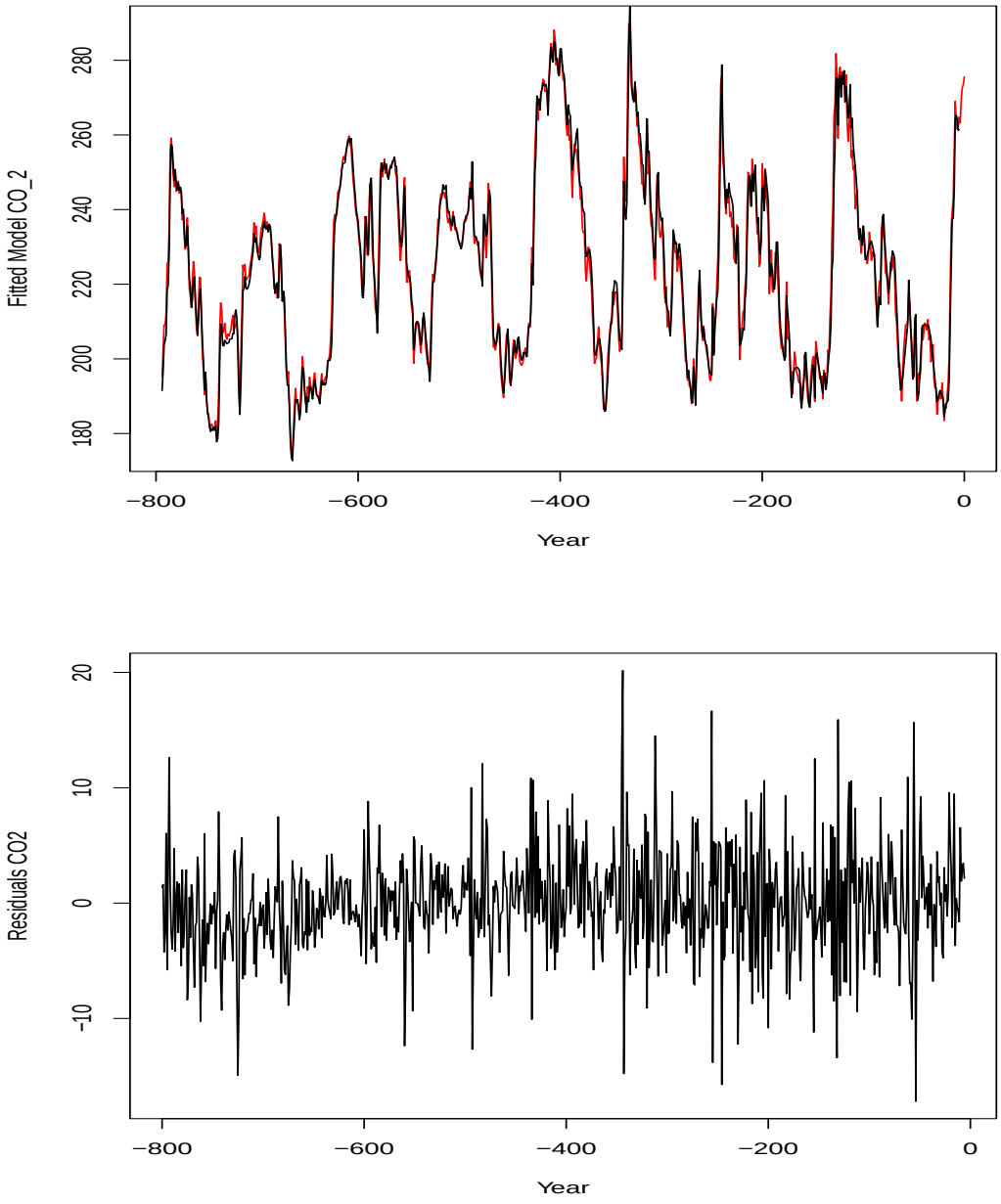

Figure 11: Original Data CO2 (black), fitted model for CO_2 (red) and regression residuals

the observation period. We start the forecasting at the last turning point of temperature and ice marked by the last local maximum and minimum respectively which was 124 thousand years ago. Therefore, we split our data into an in-sample period of 674 thousand years from the beginning of the data set to the last local maximum for temperature and the last local minimum for ice and the remaining data set which we use for forecasting. The in-sample forecasts are displayed in figure 12 where the red line is the forecast of our cyclical model. Confidence bands for our forecast are displayed as the black lines. The data for all three paleoclimate series leaves the confidence bands for the last observations. This is exactly the time where humanity appeared on earth showing the influence humanity has to the earth climate even before the beginning of the industrial time.

Our cyclical model tends to forecast the climate variables accurately most of the times. Only for the last observations we find much lower forecasted values for temperature and CO_2 and much higher forecasted

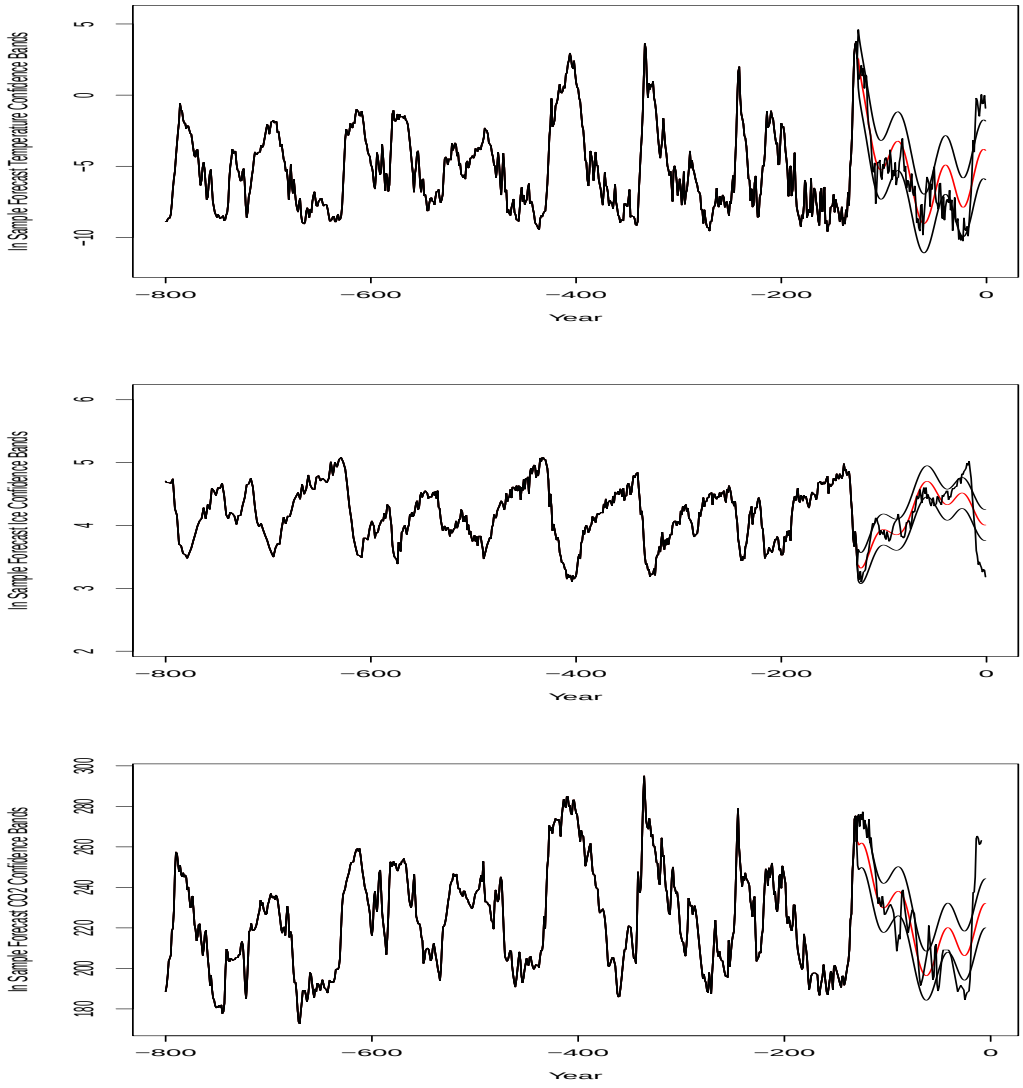

Figure 12: In Sample forecasts for the cyclical model including confidence bands

values for ice. This is the time when humanity appears on earth and obviously also in its early stage has a huge impact on the earth climate. This finding is in line with the findings of Castle and Hendry (2020) and Blazsek and Escribano (2023).

Comparing the mean squared forecasting errors of the models (see table 6) shows that our cyclical model reduces the forecasting error substantially.

	Cyclical Model	Castle and Hendry
Temperature	2.6675	3.8525
Ice	0.0286	0.0586
CO_2	148.071	238.321

Table 6: Mean Square Forecasting Error for all four regressions

To check whether this is a significant improvement in the forecasting error we applied the Diebold-Mariano test to the forecasts from our cyclical model and the Castle and Hendry model testing the null hypothesis of equal forecast accuracy. The Diebold-Mariano test rejects this null hypothesis at all levels for temperature (p-value = $1.5763x10^{-8}$), ice volume (p-value = $1.035x10^{-6}$) and CO_2 (p-value

$= 1.75x10^{-12}$). Thus, our model provides significantly better forecasts then the Castle and Hendry approach.

6.2 Forecasting Turning Points in the Climate Variables for the next 100.000 years

Castle and Hendry (2020) provide values for the earth obliquity and eccentricity for the next 100.000 years. We use our cyclical model to provide out of sample forecasts for temperature, ice and CO_2 with a forecasting horizon of $h = 100$ using all available data points. We provide forecasting including and excluding the effect of humanity. The forecasts excluding the effect of humanity are obtained by excluding the last 10.000 years from the in sample period and derive from this point a $h = 110$ step ahead forecast. The forecasts are displayed in figure 13. It can be seen that excluding the effect of humanity gives far lower forecasts for temperature and CO_2 and higher values for ice volume. The difference becomes smaller with a growing forecasting horizon. This may though be due to the long forecasting horizon also compared to the length of the in sample period.

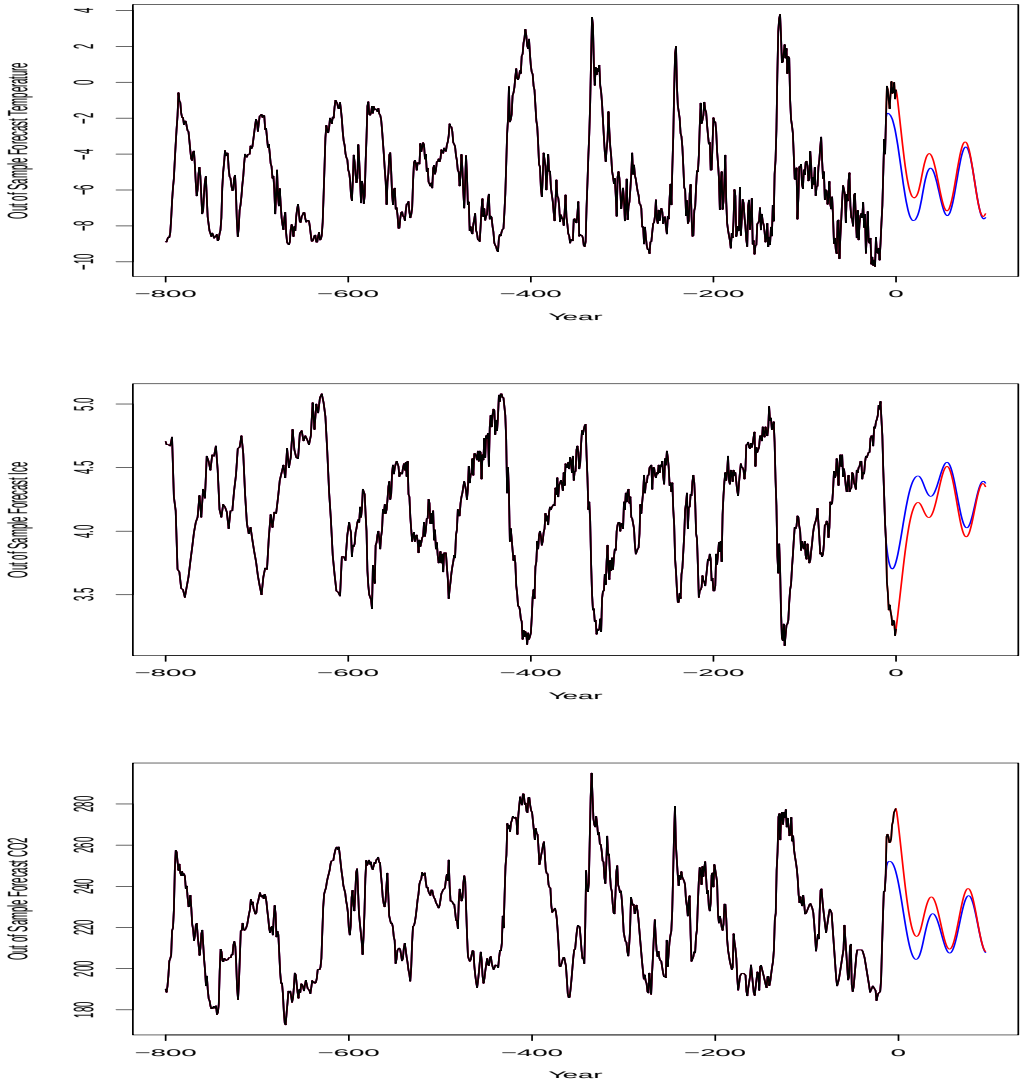

Figure 13: Out of Sample forecasts including the effect of humanity (red) and excluding the effect of humanity (blue)

Our model indicates that we are currently in a maximum for temperature and CO_2 and a minimum for ice volume and that we will have the next turning point in the coming 1000 years. This finding is in line with the findings of Blazsek and Escribano (2022). The next turning point is then estimated to be in roughly 22.000 years.

We summarize the predicted out-of sample turning points given in thousand years in table 7. We find 6 turning points which coincides for temperature and ice volume while CO_2 follows slightly behind these variables.

	TP 1	TP 2	TP 3	TP 4	TP 5	TP 6
Temperature	1	22	38	58	78	97
Ice	1	26	38	58	79	97
CO_2	2	25	41	61	81	100

Table 7: Out of sample estimated turning points (TP)

In comparison we also estimate the turning points without the effect of humanity (see table 8). It is generally assumed that humanity delays the turning point. We can confirm this for the nearest turning points which all are predicted to should have been about 8000 years ago for temperature and slightly later for ice and CO_2. Including humanity though predicts that we are currently observing a turning point. This effect is less pronounced for the next turning points which may be due to the fact that the forecasts become closer anyway with increasing forecasting horizon.

	TP 1	TP 2	TP 3	TP 4	TP 5	TP 6
Temperature	-8	20	39	57	77	97
Ice	-3	25	39	57	78	97
CO_2	-6	23	41	60	80	100

Table 8: Out of sample estimated turning points without the effect of humanity (TP)

7 Conclusion

In this paper the cyclical behaviour of paleoclimate variables is modelled. We consider data from the antarctic ice core dating back about 800.000 years of the earth temperature, the global ice volume and atmospheric carbon dioxid (CO_2) level. This data is strongly connected to exogeneous orbital variables such as the changes in the non-circularity of the Earth's orbit (eccentricity), changes in the tilt of the Earth's rotational axis relative to the ecliptic (obliquity) and the circular rotation of the rotational axis itself (precession). It is well known that these orbital variables are highly cyclical with a period of 100.000 years for eccentricity, 41.000 years for obliquity and 19.000 to 23.000 years for precession, the so-called Milankovich cycles. We investigate which of these cycles is dominant in the paleoclimate variables.

Using the model selection procedure for cyclical models of Leschinski and Sibbertsen (2019) it turns out that the 100.000 years cycle of eccentricity as well as the 41.000 years cycle of obliquity can be seen in all paleoclimate variables whereas the shorter cycle due to precession is not significant in any of the paleoclimate variables.

A cyclical cointegration analysis confirms the relation of the paleoclimate variables to eccentricity and obliquity, While the earth's temperature and the ice volume are cointegrated with obliquity at the respective cyclical frequency we find cyclical fractional cointegration for all paleoclimate variables with eccentricity at the respective frequency. It should be mentioned that for the 41.000 years cycle of obliquity

also cyclical cointegration between temperature and ice can be established while none of the paleoclimate variables are cyclically cointegrated at the 100.000 years cycle of eccentricity.

These findings are used to build a VAR(2)-type forecasting model for temperature, ice volume and CO_2 including the two relevant cycles of eccentricity and obliquity and contemporaneous and lagged values of temperature, ice volume, CO_2, obliquity and eccentricity. All of these variables enter the regression linearly. Adding nonlinear combinations as in Castle and Hendry (2020) does not improve the model fit. The new model delivers superior forecasts in terms of the MSE than the model of Castle and Hendry (2020). In addition our model indicates that the earth is currently in a turning point with a maximum of temperature and CO_2 and a minimum of ice volume with the next predicted turning point to come in 22.000 years for temperature and 26.000 years for ice volume.

Our forecasts clearly show the effect of humanity even before the industrial time. The currently observed and forecasted values are much lower for temperature and CO_2 and much higher for ice volume when excluding the effect of humanity from our forecasts.

Acknowledgements

The authors are grateful to Josu Arteche, Jennifer Castle, Liudas Giraitis, Jesus Gonzalo, David Hendry, Yeliz Ã–zer and the participants of the conference on Climate Finance in Hannover 2023, the Luxemburg Time Series Workshop 2024, the Workshop on Time Series Econometrics 2024 in Zaragossa and the IAAE 2024 in Thessaloniki for helpful comments and discussion. Tomas del Barrio Castro gratefully acknowledges financial support from project PID2020-114646RB-C430 funded by MCIN/AEI /10.13039/501100011033. Alvaro Escribano gratefully acknowledges financial support by MICIN/ AEI/10.13039/50110001 Agencia Estatal de Investigacion-Ministerio de Ciencia e Innovacion, (Maria de Maeztu); MICIN/AEI/2023/00378/001 and CEX2021-001181-M; CEX2021-001181-M financed by MICIU/AEI/10.13039/501100011033 and Comunidad de Madrid, grant EPUC3M11 (V PRICIT). Philipp SIbbertsen gratefully acknowlwdges financial support by Deutsche Forschungsgemeinschaft under grant 258395632.

References

Abadir, Karim M., Natalia Bailey, Walter Distaso, and Liudas Giraitis (2024). "Estimation of random cycles in persistent time series". In: *Working Paper, Queen Mary University*.

Arteche, Josu and Peter M Robinson (2000). "Semiparametric inference in seasonal and cyclical long memory processes". In: *Journal of Time Series Analysis* 21, pp. 1–25.

Bauwens, Luc, Guillaume Chevillon, and Sebastien Laurent (2023). "We modeled long memory with just one lag!" In: *Journal of Econometrics* 236, p. 105467.

Blazsek, Szabolcs and Alvaro Escribano (2022). "Robust estimation and forecasting of climate change using score-driven ice-age models". In: *Econometrics* 10, p. 9.

Blazsek, Szabolcs and Alvaro Escribano (2023). "Score-driven threshold ice-age models: Benchmark models for long-run climate forecasts". In: *Energy Economics* 118, p. 106522.

Castle, Jennifer and David F. Hendry (2020). *Climate Econometrics: An Overview (Foundations and Trends in Econometrics)*. Now Publishers Foundation: Hanover, USA.

Chevillon, Guillaume, Allan Hecq, and Stephane Laurent (2018). "Generating univariate fractional integration within a large VAR(1)". In: *Journal of Econometrics* 204, pp. 54–65.

Davidson, James, David B. Stephenson, and Alemtsehai A. Turasie (2015). "Time Series Modelling of Paleoclimate Data". In: *Environmetrics* 27, pp. 55–65.

Fischer, Hubertus, Martin Whalen, Jesse Smith, Derek Mastroianni, and Bruce Deck (1999). "Ice core records of atmospheric co2 around the last three glacial terminations". In: *Science* 283(5408), pp. 1712–1714.

Giraitis, L. and R. Leipus (1995). "A generalized fractionally differencing approach in long-memory modeling". In: *Lithuanian Mathematical Journal* 35(1), pp. 53–65. ISSN: 0363-1672. DOI: 10.1007/BF02337754.

Granger, Clive (1966). "The Typical Spectral Shape of an Economic Variable". In: *Econometrica* 34, pp. 150–161.

Hays J, D., John Imbrie, and N.J. Shackleton (1976). "Variations in the Earth's Orbit: Pacemaker of the Ice Ages". In: *Science* 194, pp. 1121–1132.

Hualde, Javire and Morten Nielsen (2023). "Fractional Integration and Cointegration". In: *Oxford Research Encyclopedias*. DOI: https://doi.org/10.1093/acrefore/9780190625979.013.639.

Kaufmann, Robert K. and Katarina Juselius (2013). "Testing hypotheses about glacial cycles against the observational record". In: *Paleoceanography* 28, pp. 175–184.

Leschinski, Christian and Philipp Sibbertsen (2019). "Model order selection in periodic long memory models". In: *Econometrics and Statistics* 9, pp. 78–94. ISSN: 24523062. DOI: 10.1016/j.ecosta.2017.11.002.

Mac Millan, David G. and Mark E. Wohar (2019). "The relationship between temperature and co2 emissions: Evidence from a short and very long dataset". In: *Applied Economics* 46, pp. 3683–3690.

Maslin, Mark Andrew (2016). "In Retrospect: Forty years of linking orbits to ice ages". In: *Nature* 540, pp. 208–210.

Miller, Isaak (2019). "Testing cointegrating relationships using irregular and non-contemporaneous series with an application to paleoclimate data". In: *Journal of Time Series Analysis* 40, pp. 936–950.

Mudelsee, Manfred (2001). "The phase relations among atmospheric CO2 content, temperature and global ice volume over the past 420 ka." In: *Quaternary Science Reviews* 20, pp. 583–589.

Paillard, Didier (2001). "Glacial Cycles: Toward a new paradigm". In: *Reviews of Geophysics* 39, pp. 325–346.

Proietti, Tommaso and Federico Maddanu (2024). "Modelling cycles in climate series: The fractional sinusoidal waveform process". In: *Journal of Econometrics* 239, p. 105299. DOI: https://doi.org/10.1016/j.jeconom.2022.04.008.

Reikard, Gordon (2021). "Forecasting paleoclimatic data with time series models". In: *Results in Geophysical Sciences* 6, p. 100015.

Ruddiman, William (2005). *Plows, Plagues and Petroleum: How Humans Took Control of the Climate*. Princeton University Press: Princeton.

Schennach, Susanne M. (2018). "Long memory via networking". In: *Econometrica* 86(6), pp. 2221–2248. DOI: https://doi.org/10.3982/ECTA11930.

Voges, Michelle and Philipp Sibbertsen (2021). "Cyclical fractional cointegration". In: *Econometrics and Statistics* 19, pp. 114–129.

Walker, Gilbert (1914). "On the criteria for the reality of relationships or periodicities". In: *Calcutta Ind. Met. Memo.*